PERGAMON International Journal of Multiphase Flow 24 (1998) 975–1004

International Journal of Multiphase Flow

A two-fluid model for stratified flows with curved interfaces

N. Brauner, D. Moalem Maron, J. Rovinsky

Department of Fluid Mechanics, Faculty of Engineering, Tel-Aviv Univ., Tel-Aviv, Israel

Received 2 December 1996; received in revised form 19 January 1998

Abstract

This study is motivated by the need to develop a practical tool for predicting the interface shape in stratified flow of a general two-fluid system. A configuration of a curved interface is considered.

A two-fluid model is used to solve the momentum equations for a variable interface curvature. Energy considerations provide a closure relation for the interface curvature. The analysis identifies all the input dimensionless parameters which determine the solution for the stratified flow pattern. When these are given, a complete solution of the problem is obtained, including the interface shape, *in situ* hold-up and pressure drop.

The validity of the two-fluid model is evaluated by comparing its prediction with available experimental data and with the results of exact analytical solutions for laminar flows with curved interfaces.

Thus, the conventional two-fluid model has been extended to tackle stratified flow with curved interfaces and various flow regimes, in which case analytical solutions are complicated and restricted to laminar flows.

Keywords: Two-fluid model; Stratified flow; Curved interface

1. Introduction

The stratified flow attracts continuous research efforts. It is considered a basic flow configuration in horizontal and slightly inclined two-fluid systems of a finite density differential.

The feasibility of exact analytical solutions for stratified flows is almost restricted to laminar–laminar flows which are of limited relevance to gas–liquid two phase flows. However, laminar flow in both phases is frequently encountered in liquid–liquid systems, i.e. viscous oil–water flows. Indeed, several analytical studies for laminar–laminar flow between parallel-plates (Russell & Charles, 1959; Tang & Himmelblau, 1963) and numerical solutions for circular pipe

0301-9322/98/$19.00
PII: S0301-9322(98)00005-6

geometry (Gemmell & Epstein, 1962; Charles & Redberger, 1962) were reported in literature. Analytical solutions for stratified configuration in circular geometry were attempted by Bentwich (1964) and Yu & Sparrow (1967) and recently Brauner et al. (1995); Brauner et al., 1996a,b). The latter provided analytical expressions in terms of Fourier integrals in the bipolar coordinate system for the two-dimensional velocity profiles and the distribution of shear stresses over the tube wall and free interface. The interface was considered to be either flat or curved. The interfacial curvature has been found to have a significant effect on the local and integral two-phase flow characteristics (Moalem Maron et al., 1995; Brauner et al., 1997).

The prescription of the characteristic interface curvature is required in order to initiate the solution of the flow problem and the associated transport phenomena. The vast majority of studies on stratified two-phase flows assumed a plane interface between the phases. A configuration of a plane interface is appropriate for two phase systems which are dominated by gravity, as in the case of large scale air–water systems under earth gravitation. In liquid–liquid systems with small density difference or in reduced gravity systems (even with high density difference), surface phenomena may dominate, in which case the interface is curved. Therefore, for a general two-fluid system, one should consider a curved interface as a basic configuration.

In a recent study (Brauner et al., 1996b), energy considerations have been employed to predict the interface configuration. The effects of the fluid physical properties, *in situ* hold-up, tube dimension, wall adhesion and gravitation on the characteristic interface curvature were explored. The prediction of the interface curvature provides a closure relation required for a complete solution of stratified flows with curved interfaces. When combined with the solution of the flow equations (Brauner et al., 1996a), it provides the interface configuration and the corresponding local and integral flow characteristics for a variety of laminar two-fluid systems (Brauner et al., 1995, 1997).

Due to the complex flow geometry of the stratified configuration in circular conduits, most of the models for pipe flow used the averaged two-fluid formulation. For turbulent two-phase flows or mixed flow regimes in the two-phases, the one-dimensional modeling of stratified flow is considered to be the practical tool for analyzing the integral flow characteristics, namely, pressure drop and *in situ* hold-up. However, all two-fluid models assumed a plane interface between the stratified layers (e.g. Agrawal et al., 1973; Taitel & Dukler, 1976; Wang & Charles, 1981; Brauner & Moalem Maron, 1989; Hall & Hewitt, 1993) even when these were specifically addressing the analysis of liquid–liquid systems. The interface curvature affects the fluids contact area with the tube wall. Therefore it may have a crucial effect on the flow pressure drop, particularly when the viscosity ratio is high; for example, the performance of crude-oil/water transportation lines (Russell & Charles, 1959; Charles, 1960; Charles & Redberger, 1962).

In this paper, a straightforward extension of the two-fluid model for analyzing stratified flow with curved interfaces is presented. The solution of the hydrodynamic model is combined with energy considerations to yield a complete solution for the interface configuration and the associated flow characteristics for a variety of two-fluid systems and under variable operational conditions. The validity of the model and its practical significance for analyzing stratified flows are evaluated in view of experimental data of the *in situ* flow configuration and the associated pressure drop in an oil–water system, recently reported by Valle & Kvandal (1995). Finally, the accuracy of the two-fluid model is evaluated by comparing its predictions for laminar flows

with the results of the exact solution of the Navier–Stoke equations for laminar stratified flows with curved interfaces (Brauner et al., 1995).

2. Two-fluid model for curved interfaces

Consider the stratified flow of two immiscible fluids, a and b, in horizontal or slightly inclined conduit. The flow configuration and coordinates are illustrated, as shown in Fig. 1. Clearly the lighter fluid forms the upper layer. The free interface may attain a plane or curved configuration depending on the physical properties of the fluids, solid-fluid wettability, the geometrical dimensions and the fluids hold-up.

In general, when surface effects are significant, the interface configuration tends to attain a convex or concave configuration depending on the relative wettability properties of the two fluids with the wall surface. However, when gravity is dominant, the interface approaches a plane configuration.

Polar coordinate systems are utilized for the circular geometry under consideration. In Fig. 1, ϕ represents the view angle of the interface from an arbitrary point on the upper tube wall. The view angle of the interface from a point located on the bottom wall is $\phi_0 + \pi$. The curved interface is represented by a circular segment centered at 0_1 and a view angle $\phi^* - \pi$. Note that a convex interface corresponds to $\phi^* > \pi$, while a concave interface corresponds to $\phi^* > \pi$. In particular, $\phi^* = \pi$ corresponds to the case of a plane interface with $h/R = 1 - \cos \phi_0$.

The two-phase domains are defined by:

$$\text{Upper phase: } \phi_0 < \phi < \phi^* \tag{1a}$$

$$\text{Lower phase: } \phi^* < \phi < \phi_0 + \pi \tag{1b}$$

The geometrical relationships for plane and curved interfaces, in terms of ϕ_0 and ϕ^*, are summarized in Table 1.

It is worth noting that since ϕ^* is bounded in the range of $\phi_0 \leq \phi^* \leq \phi_0 + \pi$, the maximal interface curvature for $\phi_0 \rightarrow 0$ is bounded by π, while for $\phi_0 \rightarrow \pi$ the minimal curvature is π and its maximal value is 2π.

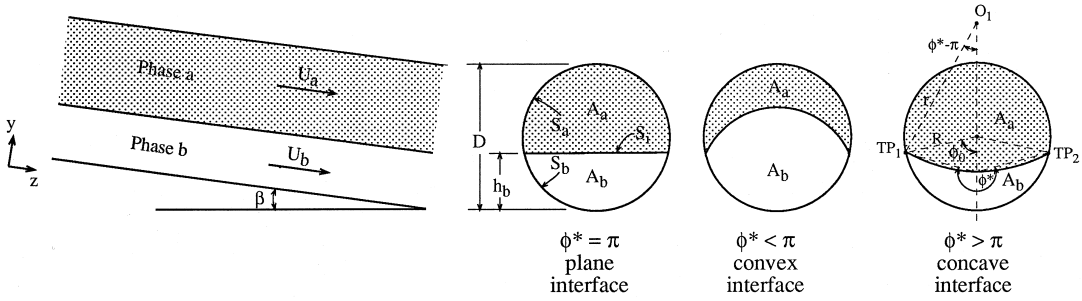

Fig. 1. Schematic description of two-phase stratified flows with curved interfaces.

Table 1
Geometrical relationships for curved and plane interfaces

	Curved interface, $\phi^* \neq \pi$	Plane interface, $\phi^* = \pi$
$\tilde{A} = \frac{A}{D^2}$	$\pi/4$	$\pi/4$
$\tilde{A}_a = \frac{A_a}{D^2}$	$\frac{1}{4}\{\pi - \phi_0 + \frac{1}{2}\sin(2\phi_0) - (\frac{\sin\phi_0}{\sin\phi^*})^2[\pi - \phi^* + \frac{1}{2}\sin(2\phi^*)]\}$	$\frac{1}{4}[\pi - \phi_0 = \frac{1}{2}\sin(2\phi_0)]$
$\tilde{A}_b = \frac{A_b}{D^2}$	$\frac{1}{4}\{\phi_0 - \frac{1}{2}\sin(2\phi_0) - \frac{\sin^2\phi_0}{\sin^2\phi^*}[\phi^* - \pi - \frac{1}{2}\sin(2\phi^*)]\}$	$\frac{1}{4}[\phi_0 = \frac{1}{2}\sin(2\phi_0)]$
$\tilde{S}_a = \frac{S_a}{D}$	$\pi - \phi_0$	$\pi - \phi_0$
$\tilde{S}_b = \frac{S_b}{D}$	ϕ_0	ϕ_0
$\tilde{S}_i = \frac{S_i}{D}$	$(\pi - \phi^*)\sin(\phi_0)/\sin(\phi^*)$	$\sin(\phi_0)$
$\tilde{\mathrm{U}}_a = \frac{\mathrm{U}_a}{U_{as}}$	$\pi/\{\pi - \phi_0 + \frac{1}{2}\sin(2\phi_0) - (\frac{\sin\phi_0}{\sin\phi^*})^2[\pi - \phi^* + \frac{1}{2}\sin(2\phi^*)]\}$	$\pi/[\pi - \phi_0 + \frac{1}{2}\sin(2\phi_0)]$
$\tilde{\mathrm{U}}_b = \frac{\mathrm{U}_b}{U_{bs}}$	$\pi/\{\phi_0 - \frac{1}{2}\sin(2\phi_0) + (\frac{\sin\phi_0}{\sin\phi^*})^2[\pi - \phi^* + \frac{1}{2}\sin(2\phi^*)]\}$	$\pi/[\phi_0 - \frac{1}{2}\sin(2\phi_0)]$

Assuming a fully developed flow, the integral forms of the momentum equations for the two fluids are:

$$-A_a\left(\frac{\mathrm{d}p}{\mathrm{d}z}\right) - \tau_a S_a - \tau_i S_i + \rho_a A_a g \sin\beta = 0 \tag{2a}$$

$$-A_b\left(\frac{\mathrm{d}p}{\mathrm{d}z}\right) - \tau_b S_b + \tau_i S_i + \rho_b A_b g \sin\beta = 0 \tag{2b}$$

Eliminating the pressure drop yields:

$$\tau_a \frac{S_a}{A_a} - \tau_b \frac{S_b}{A_b} + \tau_i S_i\left(\frac{1}{A_a} + \frac{1}{A_b}\right) + (\rho_b - \rho_a) g \sin\beta = 0. \tag{3}$$

Obviously, exact computation of the shear stresses is limited either to laminar flows or simple geometries, and yet is complicated. Thus, the more conventional way to evaluate the wall and interfacial shear stresses is to adopt the Blasius equation, whereby wall and interfacial shear stresses (τ_a, τ_b, τ_i) are expressed in terms of the phases velocity heads and appropriate friction factors, f_a, f_b, f_i:

$$\tau_a = f_a \rho_a \mathrm{U}_a^2/2; \quad f_a = \mathrm{C}_a\left(\frac{D_a \mathrm{U}_a}{\nu_a}\right)^{-\mathrm{n}_a} \tag{4a}$$

$$\tau_b = f_b \rho_b \mathrm{U}_b^2/2; \quad f_b = \mathrm{C}_b\left(\frac{D_b \mathrm{U}_b}{\nu_b}\right)^{-\mathrm{n}_b}. \tag{4b}$$

$$\tau_i = f_i \rho \frac{(\mathrm{U}_a - \mathrm{U}_b)|\mathrm{U}_a - \mathrm{U}_b|}{2} \tag{4c}$$

The Blasius type friction factor correlations, although originally derived for single phase pipe flow, have been widely used in two-phase flow models to represent the average wall and interfacial shear stresses in plane stratified flows (zero interfacial curvature) and annular flows (curved free interface). Their applicability to model stratified flow with curved (or plane) interfaces is assessed in Section 6, where the results of the two-fluid model for laminar flows are compared with the exact solutions.

In Eqs. (4a)–(c) the Reynolds numbers for the two fluids are based on the equivalent hydraulic diameters, which are defined according to the relative velocity of the phases:

$$D_a = \frac{4A_a}{(S_a + S_i)};\ D_b = \frac{4A_b}{S_b};\ \rho = \rho_a \text{ and } f_i = f_a \text{ for } U_a > U_b \tag{5a}$$

$$D_a = \frac{4A_a}{S_a};\ D_b = \frac{4A_b}{(S_b + S_i)};\ \rho = \rho_b \text{ and } f_i = f_b \text{ for} U_b > U_a. \tag{5b}$$

$$D_a = \frac{4A_a}{S_a};\ D_b = \frac{4A_b}{S_b};\ \tau_i \simeq 0 \text{ for } U_a \simeq U_b. \tag{5c}$$

Note that in horizontal gas–liquid flows, the gas velocity is of a higher order of magnitude and therefore the interface is considered as a free surface with respect to the liquid and as a stationary surface with respect to the fast gas phase (e.g. Agrawal et al., 1973). In liquid–liquid systems, the velocites of the two phases are usually of comparable levels with one phase velocity exceeding the other, depending on the fluids properties, system inclination and operational conditions. Therefore, an *adjustable* definition of the equivalent hydraulic diameters D_a, D_b ought to be adopted as part of the solution procedure (Brauner & Moalem Maron, 1989). The constants C_a, C_b, n_a, n_b in Eqs. (4a)–(b) are chosen according to the flow regime in each phase. (C = 16, n = 1 for laminar flow and C = 0.046, n = 0.2 for turbulent flow.) Clearly, the two phases in stratified flow may result in laminar–laminar (L–L), laminar–turbulent (L–T), turbulent–laminar (T–L), or turbulent–turbulent (T–T) regimes.

Introducing non-dimensional variables (designated by a tilde (˜), as defined in Table 1), and substituting Eqs. (4a)–(c) and Eqs. (5a)–(c) into Eq. (3), yields the following normalized forms of Eq. (3):

$$(\tilde{D}_a\tilde{U}_a)^{-n_a}\tilde{U}_a^2\left[\frac{\tilde{S}_a}{\tilde{A}_a} + \left(1 - \frac{1}{\tilde{Q}}\frac{\tilde{U}_b}{\tilde{U}_a}\right)^2 \tilde{S}_i\left(\frac{1}{\tilde{A}_a} + \frac{1}{\tilde{A}_b}\right)\right] - \chi^2\left[(\tilde{D}_b\tilde{U}_b)^{-n_b}\tilde{U}_b^2\frac{\tilde{S}_b}{\tilde{A}_b}\right] + 4Y = 0;\quad \tilde{Q}\tilde{U}_a/\tilde{U}_b > 1; \tag{6a}$$

$$\tilde{U}_a^2\left[(\tilde{D}_a\tilde{U}_a)^{-n_a}\frac{\tilde{S}_a}{\tilde{A}_a} - \chi^2\tilde{Q}^2(\tilde{D}_b\tilde{U}_b)^{-n_b}\left(1 - \frac{1}{\tilde{Q}}\frac{\tilde{U}_b}{\tilde{U}_a}\right)^2 \tilde{S}_i\left(\frac{1}{\tilde{A}_a} + \frac{1}{\tilde{A}_b}\right)\right] - \chi^2\left[(\tilde{D}_b\tilde{U}_b)^{-n_b}\tilde{U}_b^2\frac{\tilde{S}_b}{\tilde{A}_b}\right] + 4Y = 0;\quad \tilde{Q}\tilde{U}_a/\tilde{U}_b < 1; \tag{6b}$$

$$\chi^2(\tilde{D}_b\tilde{U}_b)^{-n_b}\tilde{U}_b^2\frac{\tilde{S}_b}{\tilde{A}_b}-(\tilde{D}_a\tilde{U}_a)^{-n_a}\tilde{U}_a^2\frac{\tilde{S}_a}{\tilde{A}_a}-4Y=0;\quad \tilde{Q}\tilde{U}_a/\tilde{U}_b\simeq 1 \tag{6c}$$

The two-phase flow parameters χ^2, Y and $\tilde{Q}$ evolve through the normalization of Eq. (3) and are given by:

$$\chi^2=\frac{4C_b/D(U_{bs}D/\nu_b)^{-n_b}\rho_bU_{bs}^2/2}{4C_a/D(U_{as}D/\nu_a)^{-n_a}\rho_aU_{as}/2}=\frac{(dp/dz)_{bs}}{(dp/dz)_{as}} \tag{7a}$$

$$Y=\frac{(\rho_b-\rho_a)g\ \sin\ \beta}{4C_a/D(U_{as}D/\nu_a)^{-n_a}\rho_aU_{as}^2/2}=\frac{(\rho_b-\rho_a)g\ \sin\ \beta}{(dp/dz)_{as}} \tag{7b}$$

$$\tilde{Q}=\frac{Q_a}{Q_b}=\frac{U_{as}}{U_{bs}} \tag{7c}$$

As shown in Table 1, the various geometric parameters and the non-dimensional velocities $\tilde{U}_a$, $\tilde{U}_b$ are all functions of the phases distribution angle over the tube wall, ϕ_0 and the interface curvature ϕ^*. Hence, given the flow regime in the two-layers ($C_{a,b}$ and $n_{a,b}$ are prescribed), the general relation stated by Eqs. (6a)–(c) is:

$$f(\chi^2,\tilde{Q},\ Y,\ \phi^*,\ \phi_0)=0 \tag{8}$$

The Martinelli parameter χ^2 incorporates the fluids physical properties $\tilde{\mu}=\mu_a/\mu_b$, $\tilde{\rho}=\rho_a/\rho_b$. In particular, for horizontal laminar (L–L) flows, $Y=O$, $\chi^2=(\tilde{\mu}\tilde{Q})^{-1}$, the solution of Eqs. (6a)–(c) yields:

$$\phi_0=\phi_0(\tilde{Q},\ \tilde{\mu},\ \phi^*);\quad L_{(a)}-L_{(b)}, \tag{9a}$$

while for horizontal turbulent (T–T) flows the solutions of Eqs. (6a)–(c) is also dependent on fluids density ratio, whereby:

$$\phi_0=\phi_0(\tilde{Q},\ \tilde{\mu},\ \tilde{\rho},\phi^*);\quad T_{(a)}-T_{(b)} \tag{9b}$$

For mixed flow regime in the two layers, the relationships which evolve from Eqs. (6a)–(c) with the corresponding expression for χ^2 (Eq. (7a)) are:

$$\text{or}\quad \left.\begin{array}{l}\phi_0=\phi_0(\tilde{Q},\ Re_{bs},\ \tilde{\mu},\ \phi^*)\\ \phi_0=\phi_0(\tilde{Q},\ Re_{as},\ \tilde{\mu},\tilde{\rho},\ \phi^*)\end{array}\right\}L_{(a)}-T_{(b)} \tag{10a}$$

$$\text{or}\quad \left.\begin{array}{l}\phi_0=\phi_0(\tilde{Q},\ Re_{as},\ \tilde{\mu},\ \phi^*)\\ \phi_0=\phi_0(\tilde{Q},\ Re_{bs},\ \tilde{\mu},\tilde{\rho},\ \phi^*)\end{array}\right\}L_{(b)}-T_{(a)} \tag{10b}$$

Given a two-fluid system ($\tilde{\mu}$, $\tilde{\rho}$), the solutions defined by Eqs. (9a)–(b) can be represented by 'flow monograms' as in Fig. 2. Each point along a curve of a specified $\tilde{Q}$ represents a possible combination of (ϕ^*, ϕ_0). The values of both are required for determining the *in situ* flow configuration. Once the interface curvature is prescribed (as in the case of plane interface), the phases distribution angle ϕ_0 for specific operational conditions ($\tilde{Q}$) can be extracted from the

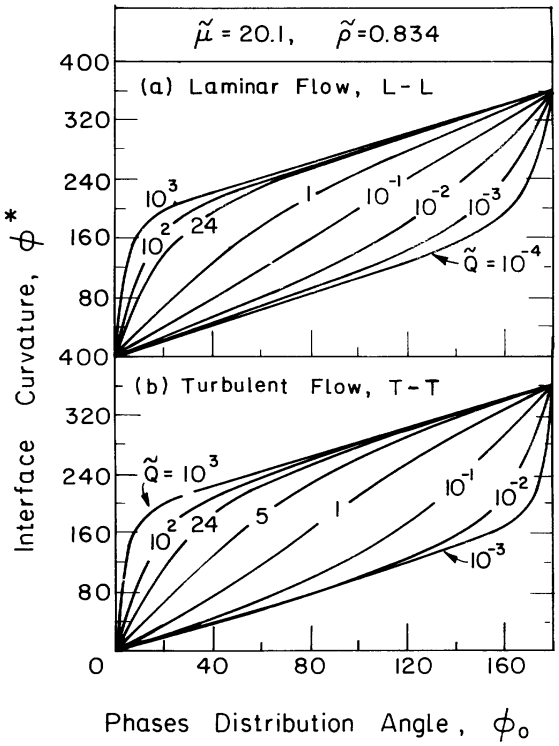

Fig. 2. Flow monograms: effect of phases flow rates. (a) laminar–laminar flow; (b) turbulent–turbulent flow.

corresponding flow monogram for either laminar flows (Fig. 2a) or turbulent flows (Fig. 2b). Note that in view of Eq. (9a), the flow monograms for laminar flows are independent of the fluids density ratio. Both for laminar and turbulent two-phase flows, the flow monograms of a two-fluid system (specified $\tilde{\rho}$ and $\tilde{\mu}$) are uniquely determined by the fluids flow rate ratio $\tilde{Q}$. For mixed flow regimes, (either laminar(a)–turbulent(b) or turbulent(a)–laminar(b)) more detailed information is required. In view of Eqs. (10a)–(b) both Q_a and Q_b should be specified for constructing the corresponding flow monogram. This detailed information is also needed for constructing the flow monograms for inclined systems, $Y \neq O$ with all possible combinations of phases flow regimes.

In order to follow the effects of laminar/turbulent flow regime transitions on the flow monogram, it is useful to refer to particular flow rates ratio which results in simultaneous L–T transition in both phases (when increasing flow rates while maintaining $\tilde{Q}$). This may happen when $Re_{as} \simeq Re_{bs}$, or $\tilde{Q} = \tilde{Q}_{IP} = \tilde{\mu}/\tilde{\rho} = \tilde{\nu}$ ($=24$ for the two fluids in Fig. 2), in which case the Martinelli parameter remains invariant with flow regime transition, $\chi^2_{IP} = \tilde{\rho}/\tilde{\mu}^2$. Along $\tilde{Q} \ll \tilde{Q}_{IP}, (\chi^2)_{T-T} > (\chi^2)_{L-L}$, when both phases flow rates is increased, the lower phase becomes turbulent first, in which case the laminar turbulent transition is associated with an increase of the lower phase hold-up. Hence, using $\tilde{Q} \ll \tilde{Q}_{IP}$ and a particular $\phi^*, (\phi_0)_{T-T} > (\phi_0)_{L-L}$. This trend is indicated in Fig. 2, by comparing the corresponding flow curves for L–L and T–T regimes obtained for $\tilde{Q} \ll \tilde{Q}_{IP} = 24$. This is vice versa for $\tilde{Q} \gg \tilde{Q}_{IP}$. Then, $(\chi^2)_{T-T} < (\chi^2)_{L-L}$ and therefore $(\phi_0)_{T-T} < (\phi_0)_{L-L}$. The effects of the flow regime on the characteristics of the solutions

obtained via the two-fluid model for plane interface ($\phi^* = \pi$) were detailed in Brauner & Moalem Maron (1989).

It is to be noted that the literature for gas–liquid systems, following the Lockhart and Martinelli approach, emphasizes the role of χ^2 as the sole parameter. In the case of horizontal gas–liquid flows, when the gas velocity is characteristically much greater than the liquid phase velocity, the two-liquid model equations are reduced to a single parameter equation and the *in situ* hold-up and pressure drop are determined by the Martinelli parameter. However, in general two-fluid systems (in particular liquid–liquid systems), the velocities of the two-phases may be of comparable levels, and therefore the flow characteristics of two-fluid systems are dependent on the two parameters, χ^2 and $\tilde{Q}$. In L–L flows, the equivalent two-parameters are the viscosities ratio and the flow rates ratio. Therefore, the L–L flow monograms (Fig. 2a) can, in principle, be arranged in terms of $\tilde{\mu}\tilde{Q}$, in which form the range of a single parameter solution appears. The range of validity of single-parameter solutions was studied by Brauner et al. (1995); Brauner et al., 1996a) with regard to the exact solutions of the 2-D laminar flow equations. It was concluded that for two-fluid systems of comparable viscosities, both parameters $\tilde{\mu}$ and $\tilde{Q}$ are required. However, in the extreme of $\tilde{\mu} > 100$ or $\tilde{\mu} < 0.01$, L–L flow monograms of various $\tilde{Q}$ follow a uniform curve of ϕ^* vs. ϕ_0, provided they correspond to the same specified Martinelli parameter. For instance, a L–L flow monogram obtained for $\tilde{\mu} = 0.01$ is practically valid for any $\tilde{\mu} \leq 0.01$ when curves of constant $\tilde{Q}$ are considered in terms of the corresponding $\tilde{\mu}\tilde{Q}$. Similarly, the results for $\tilde{\mu} \gg 1$ can be extracted from those obtained for $\tilde{\mu} = 100$.

Having obtained a solution for ϕ_0 at a particular ϕ^* from the flow monogram, the *in situ* flow configuration is determined from the geometrical relationships in Table 1. The system pressure drop is obtained by eliminating τ_i using Eqs. (1a)–(b). In a dimensionless form:

$$\frac{\mathrm{d}\tilde{P}_a}{\mathrm{d}Z} = \frac{\mathrm{d}p/\mathrm{d}z}{(\mathrm{d}p/\mathrm{d}z)_{as}} = \frac{1}{4}\chi^2 \mathrm{U}_b^2 (\tilde{D}_b \mathrm{U}_b)^{-\mathrm{n}_b} \frac{\tilde{S}_b}{(\tilde{A}_b + \tilde{A}_a)} + \frac{1}{4}(\tilde{D}_a \mathrm{U}_a)^{-\mathrm{n}_a} \mathrm{U}_a^2 \frac{\tilde{S}_a}{(\tilde{A}_b + \tilde{A}_a)} - \tilde{\rho} Y \tag{11a}$$

or

$$\frac{\mathrm{d}\tilde{P}_b}{\mathrm{d}Z} = \frac{\mathrm{d}p/\mathrm{d}z}{(\mathrm{d}p/\mathrm{d}z)_{bs}} = \frac{(d\tilde{P}_a/\mathrm{d}z)}{\chi^2} \tag{11b}$$

where:

$$\tilde{\rho} = \frac{\rho_a \tilde{A}_a + \rho_b \tilde{A}_b}{(\tilde{A}_a + \tilde{A}_b)(\rho_b - \rho_a)}. \tag{11c}$$

Thus, it is clear that in order to define the flow geometry and proceed in solving the flow problem for a particular two-phase system and operational conditions, the interface curvature ought to be prescribed.

3. Prediction of the interface curvature

The characteristic curvature of the two fluids interface can be predicted by employing energy considerations.

In a recent study (Brauner et al., 1996b), the variation of the potential energy, ΔE_p and surface energies ΔE_s associated with changing the interface curvature, have been explored. It was shown that the interface curvature corresponds to the minimum of the total system energy. The procedure for constructing the 'interface monogram', which yields the interface curvature as a function of ϕ_0, is briefly outlined below.

Taking the configuration of plane interface as a reference, the curving of the interface to either concave or convex shape is associated with an elevation of the system center of gravity, thereby increasing the potential energy. It also results in a change of the phases contact area with the tube wall and the phases interfacial area, resulting in a change of the system surface energies.

For an inclined conduit the change in the total system energy, ΔE (per tube length L) associated with the process of curving the interface from its otherwise planar shape, is given by Brauner et al. (1996b):

$$\begin{aligned}\frac{\Delta\tilde{E}}{\mathrm{L}} &= \frac{\Delta E}{[R^3\mathrm{L}(\rho_b-\rho_a)g\cos\beta]} = \frac{1}{\mathrm{L}}(\Delta\tilde{E}_p+\Delta\tilde{E}_s)\\ &= \left[\frac{\sin^3\phi_0}{\sin^2\phi^*}(ctg\phi^*-ctg\phi_0)\left(\pi-\phi^*+\frac{1}{2}\sin(2\phi^*)\right)+\frac{2}{3}\sin^3\phi_0^P\right]\\ &\quad+\epsilon_v\left[\sin\phi_0\frac{\pi-\phi^*}{\sin\phi^*}-\sin\phi_0^P+\cos\alpha(\phi_0^P-\phi_0)\right]\end{aligned} \tag{12a}$$

where α is the phases wettability angle with the wall and ϵ_v is the Eötvös number,

$$\epsilon_v = \frac{2\sigma_{ab}}{(\rho_b-\rho_a)g\cos\beta\ R^2} \tag{12b}$$

Given an *in situ* hold-up, $\tilde{A}_a$ (or $\tilde{A}_b$) the geometrical relationships (Table 1) yield the corresponding ϕ_0 for either plane configuration ($\phi_0^P=\phi_0(\phi^*=\pi)$) or for a curved interface with any specified ϕ^*. Hence, Eqs. (12a)–(b) with Table 1 yields the change in the total system energy associated with curving the interface to the specified ϕ^*, $\Delta\tilde{E}(\phi^*)$. The ultimate interface configuration is obtained at the particular curvature, ϕ_m^*, for which the system total energy is at its minimum. Thus, by minimizing Eqs. (12a)–(b) the steady interface curvature can be predicted for a variety of two-fluid systems of a given density difference, surface tension, gravity conditions and tube diameter. These are all embodied in the single non-dimensional Eötvös number, ϵ_v, and in terms of the relative wettability of the phases with the tube wall, as represented by cos α. The so-obtained 'optimal' interface curvature is used to construct the interface monograms shown in Figs. 3 and 4, which yield the characteristic interface curvature as a function of the phases distribution angle ϕ_0 for various Eötvös numbers and phases relative wettability.

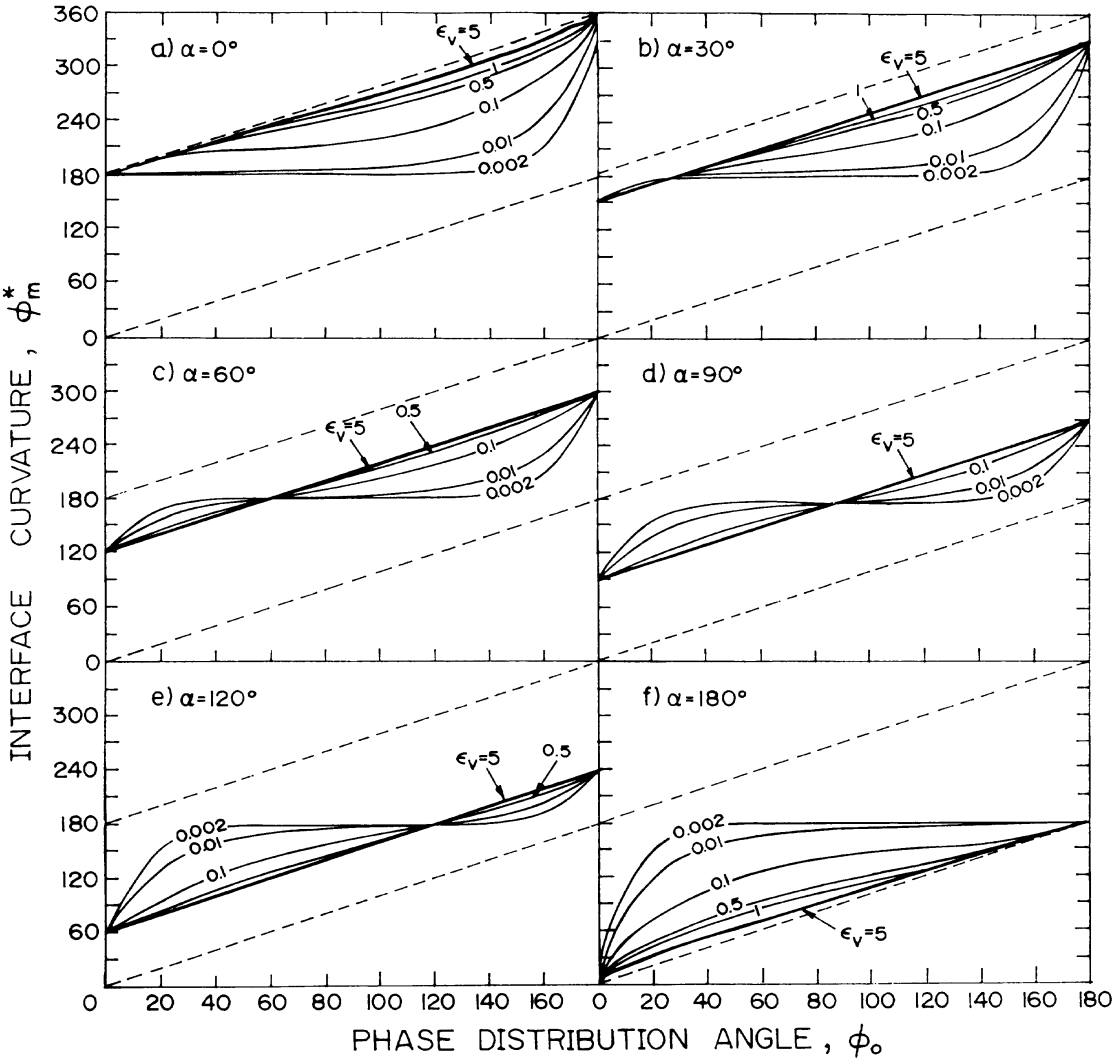

Fig. 3. Interface monograms: effect of Eötvös number for two-phase systems with various wettability angle.

Inspection of the interface monograms in Figs. 3 and 4 shows that in gravity dominated systems, $\epsilon_v \to 0$, the interface stabilizes at a planar configuration, $\phi_m^* \to \pi$ over a wide range of ϕ_0. It is to be noted that for $\epsilon_v \equiv 0$ (no surface effects) a plane interface configuration corresponds to the minimal of the system (potential) energy, irrespective of the phases hold-up (or ϕ_o). However, for small finite ϵ_v numbers and low hold-up of the non-wetting phase, the interface curvature deviates from $\phi^* = \pi$ (the non-wetting phase tends to form a 'bubble'). As surface tension effects increase, a curved interface with either concave ($\phi_m^* > \pi$) or convex ($\phi_m^* < \pi$) shape is obtained for a wider range of *in situ* hold-up.

The other extreme, corresponding to two-phase systems dominated by surface effects, $\epsilon_v \gg 1$, is shown in Fig. 4(f). For high Eötvös number, the solution for the steady interface curvature follows a straight line:

$$\phi_m^* = (180^\circ - \alpha) + \phi_0 \tag{13}$$

Thus, when $\epsilon_v \gg 1$ and $\alpha = 0$ (ideal wettability of the lower phase), the solution for ϕ_m^* coincides with the upper bound of the solution domain (see Eq. (1b)) and for $\alpha = 180^\circ$ (ideal wettability of the upper phase) ϕ_m^* follows the lower bound of the solution domain (see Eq. (1a)). In both cases, the interface configuration corresponds to a fully eccentric bubble of the non-wetting phase, irrespective of the phase hold-up. However, for $\epsilon_v \gg 1$, with $0 < \alpha < \pi$ (none of the phases ideally wets the wall), the interface configuration depends both on α and ϕ_0 (or the hold-up).

It is to be emphasized that although intuition may lead one to believe that a curved interface is typical only to small diameter (capillary) tubes, the analysis indicates that diameter effect is

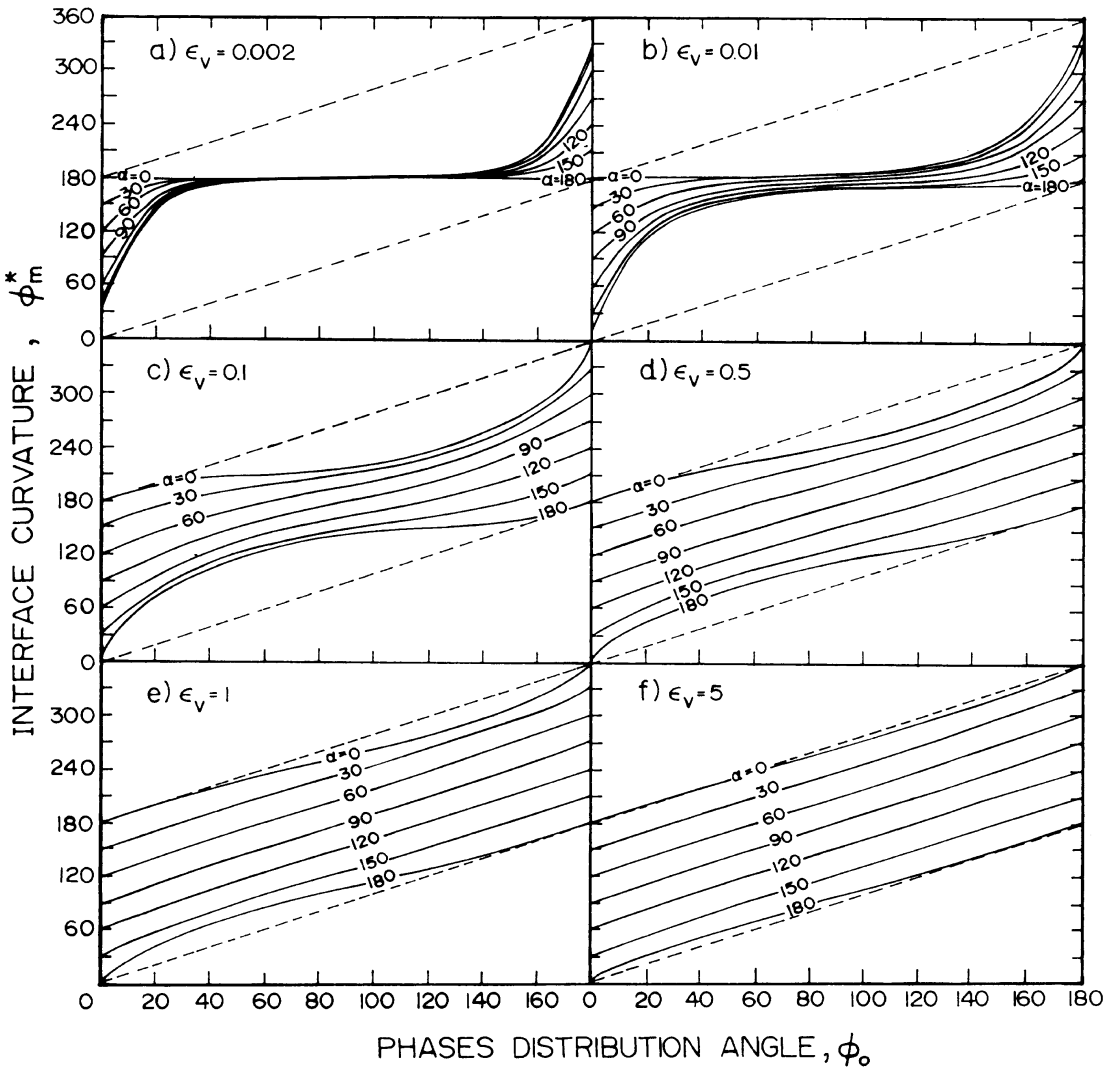

Fig. 4. Interface monograms: effect of wall adhesion for various Eötvös numbers.

embodied in the nondimensional Eötvös number. Therefore, large scale systems with two fluids of low density differential, will have the same characteristic interface curvature as capillary systems of high density differential (with identical ϵ_v and α).

In a two-phase flow system, the phases *in situ* hold-up is determined by the solution of the flow problem. This form of interface monograms, as presented in Figs. 3 and 4, can be conveniently combined with the solution of the flow problem to yield both the interface configuration and the two phase flow characteristics.

4. Construction of the system 'operational monogram'

The prediction of the interface curvature ϕ^* ought to be an integral part of the complete stratified flow solution. The basic input required for solving a stratified flow problem includes the two fluids properties (densities, viscosties and surface tension), the flow rates, tube diameter and inclination and the wall/fluids relative wettability. This information is used to calculate the relevant non-dimensional parameters needed to construct the system 'interface monogram' (in terms of ϵ_v number and wettability angle α) and the system 'flow monogram'. As discussed in Section 2, the number of non-dimensional parameters which define the flow monogram (obtained via the solution of the hydrodynamic model) depends on the flow regime in both phases and on whether a horizontal or an inclined system is considered.

The combination of the system interface monogram with the system 'flow monogram' yields the system 'operational monogram'. The construction of the 'operational monogram' is demonstrated in Fig. 5a for horizontal laminar–laminar flows and in Fig. 5b for turbulent–turbulent flows. Each intersection point of a flow curve with an interface curve on the operational monogram yields both ϕ^* and ϕ_0 for the particular two-phase system (working fluids, tube material and geometry) at the specified operational conditions (flow rates). The dashed line in Fig. 5 represents the solution ϕ_0^P obtained when imposing the assumption of a plane interface, which is a valid solution for systems with $\epsilon_v \equiv 0$. The discrepancy between the solution obtained for ϕ_0 and ϕ_0^P indicates the different flow configuration predicted for systems of non-vanishing Eötvös numbers. For $\epsilon_v = 0.1$ and ideal wettability of the lower-phase, $\alpha = 0$, the discrepancy between (ϕ^*, ϕ_0) and (π, ϕ_0^P) is already significant for high $\tilde{Q} = Q_a/Q_b$ ratios and becomes more and more dramatic for lower $\tilde{Q}$ ratios. Another noteworthy point demonstrated in Fig. 5a and Fig. 5b is that for a given physical system a wide range of interfacial curvatures may result with varying the phases input flow rates ratio. Comparison of Fig. 5a and Fig. 5b shows that for $\tilde{Q} < \tilde{Q}_{IP}$; $(= 2.85)$ and $\alpha = 0$, the transition from laminar to turbulent two-phase flow is associated with a tendency of the interface to form a more concave shape with an increased contact area between the wetting phase and the tube wall (both ϕ_0 and ϕ^* increase). Note that typical oil–water laboratory systems, with $\Delta\rho = \rho_b - \rho_a \simeq 0.1 \div 0.2$ gr/cm^3, $D = 1/2 - 2''$ and $\sigma_{ab} = 25 \div 40$ *dyne/cm*, correspond to $\epsilon_v \simeq 0.5 \div 2$. However, systems of lower density differential and much higher ϵ_v numbers are common in liquid–liquid systems, vapor–liquid systems operating near the critical point or reduced gravity systems. Obviously, with the increasing ϵ_v number, the deviation of the solution obtained for the *in situ* flow configuration (ϕ^*, ϕ_0) from the solution obtained with a plane interface (π, ϕ_0^P) increases.

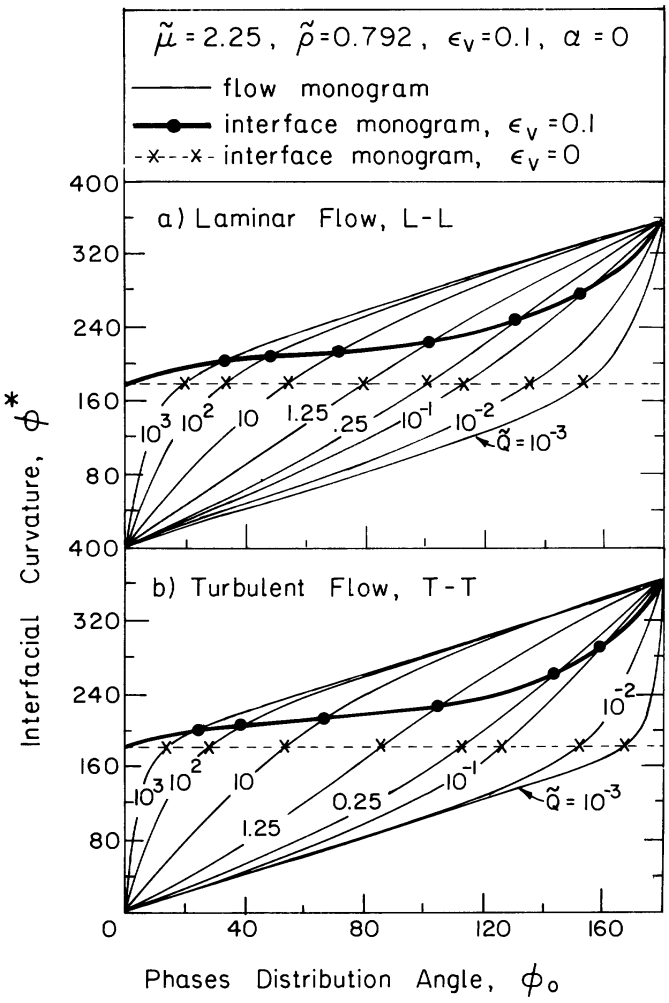

Fig. 5. Operational Monograms: effect of phases flow rates and flow regime.

Fig. 6a shows for $\epsilon_v \gg 1$ and ideal wettability of either of the phases $\alpha = 0$, or $\alpha = 180°$), the only solution for the *in situ* configuration is a fully eccentric 'bubble' of the non-wetting phase. When $\alpha = 0$, the lighter non-wetting phase forms a 'bubble' touching the upper tube wall ($\phi_0^* = 360°$, $\phi_0 = 180°$), while for $\alpha = 180°$ the heavier non-wetting phase forms a 'bubble' touching the tube bottom. These are the only solutions obtained for the problem; irrespective of the phases flow rates, flow regime or fluids viscosities. However, for partial wettability, $0 < \alpha < 180°$, the flow configuration does not necessarily correspond to the bubbly flow, even in the limit of $\epsilon_v \to \infty$. The wall/phases adhesion properties may affect stratification of the flow, whereby the interface shape (convex or concave) and the resulting contact areas of the phases with the tube wall depends on the wettability angle, flow rates and fluids properties.

The effect of the fluids viscosity in laminar flows is demonstrated in Fig. 6b indicating a variability of the characteristic interfacial curvature due to this fluid property. For a finite

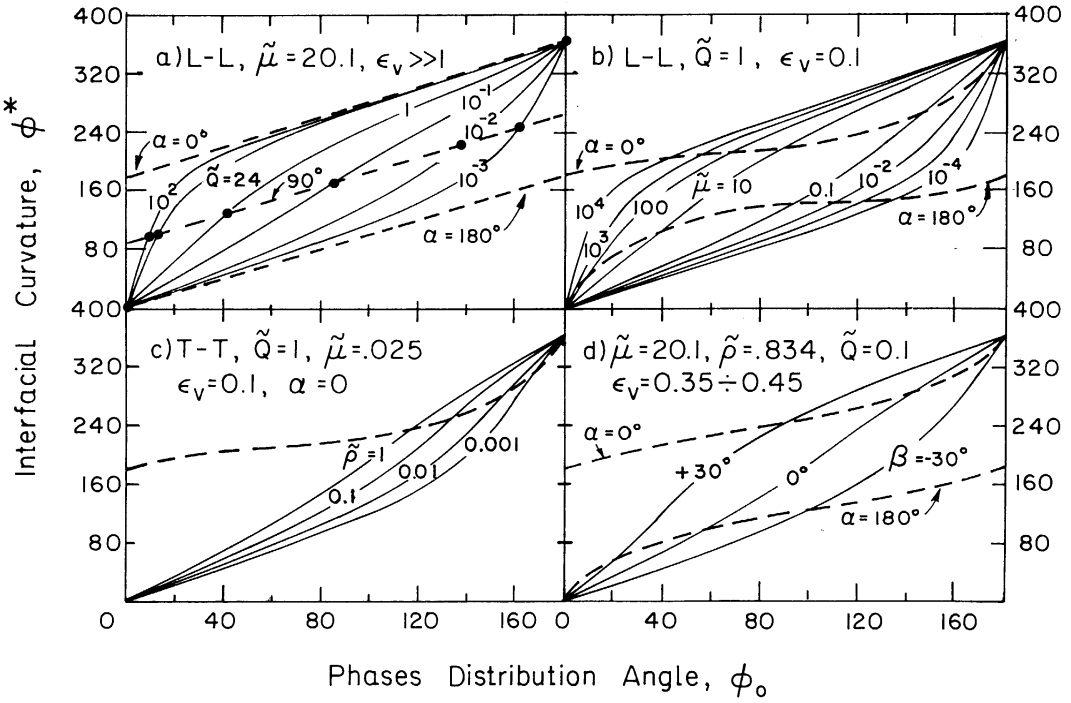

Fig. 6. Effects of various system parameters on the operational monogram.

Eötvös number, the interfacial curvature decreases as the viscosity of the non-wetting phase increases. For $\alpha = 0$, the interface is less concave and the contact area of the lubricating wetting phase with the wall decreases as $\tilde{\mu}$ increases, whereas for $\alpha = 180°$ the interface becomes more convex for higher $\tilde{\mu}$. For turbulent flows, the effect of the viscosity ratio on the flow monogram (hence, on the interface shape) is much less pronounced.

In laminar flows, the flow monograms are independent of the fluids densities while the solution of the flow problem is affected by the phases density differential only through its effect on the interface monogram. This implies that the effect of reduced gravity field on the interface configuration in laminar flows can be simulated by studying liquid–liquid systems of reduced density differential under earth gravitation. In turbulent flows, however, both the flow monogram and the interface monogram vary with $\tilde{\rho}$.

Fig. 6c shows that the variation of the flow monogram with the fluids' densities in T–T flows moderates the changes in the interface configuration affected by the variation of the interface monogram. For constant Eötvös number (and $\alpha = 0$) the interface curvature increases with a reduction in $\tilde{\rho}$. Obviously, a constant ϵ_v requires that the reduction of $\tilde{\rho}$ is accompanied by a corresponding reduction of either the tube size or gravity field.

Finally, the effect of the tube inclination on the interface configuration is demonstrated in Fig. 6d for the oil–water system studied by Russel et al. (1959). In constructing the flow monograms, the flow regime in each phase was determined according to the operational conditions resulting in turbulent water with either laminar or turbulent oil. It is shown that for ideal wettability of water, $\alpha = 0$ surface effects become more pronounced, whereby the

interface is more concave with inclining the tube upwards. However, when the oil is the wetting phase ($\alpha = 180^\circ$), the interface attains a more convex shape (ϕ^* decreases) for downward inclinations.

Having obtained the interface configuration (both ϕ_0 and ϕ^*) from the system operational monogram (e.g. Figs. 5 and 6), all other flow characteristics can be obtained via the geometrical relationships in Table 1 and the solution of the flow problem as detailed in Section 2.

5. Comparison with experimental data

The significance of considering the interfacial curvature, while modeling stratified flows of liquid–liquid systems, is demonstrated by referring to experimental data reported by Valle & Kvandal (1995). They used oil (Exxol D80) and water (with 1% NaCl) in a horizontal glass pipe of 37.5 mm ID. The Eötvös number for this system is $\epsilon_v = 0.1$ and for ideal wettability of the glass tube by the water phase, $\alpha = 0$. The pressure drop as well as the phases *in situ* distribution were measured. The *in situ* phases distribution was characterized by measuring the extent of water climbing along the tube wall, H_f and the oil–water distribution along the tube meridian (see schematic description in Fig. 7, reproduced from Valle & Kvandal, 1995). In the framework of the two-fluid model presented in Section 2, H_f is given by:

$$\tilde{H}_f = \frac{H_f}{D} = 0.5(1 - \cos\ \phi_0) \tag{14a}$$

The experimental value of H_{50} has been identified as the location of the oil/water interface along the meridian, which is then given by:

$$\tilde{H}_{50} = \frac{H_{50}}{D} = 0.5\left[1 - \cos\phi_0 + \sin\ \phi_0\ ctg\left(\frac{\phi^*}{2}\right)\right] \tag{14b}$$

The predicted *in situ* flow configuration as a function of oil and water flow rates ratio is given in Fig. 8. The figure has been constructed based on the laminar–laminar and turbulent–turbulent operational monograms of this particular two-fluid system. Given the input flow

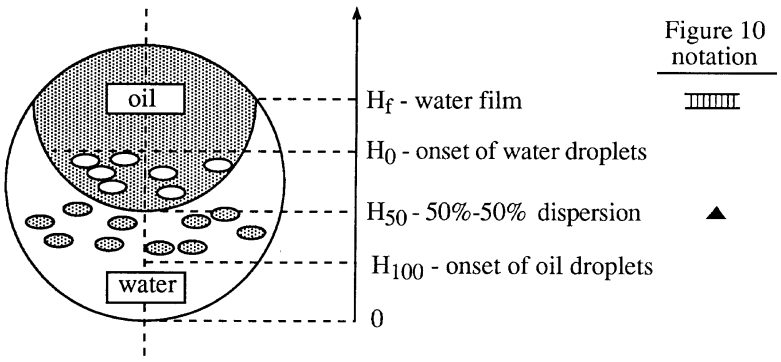

Fig. 7. Definition of the terminology used in Valle and Kvandal (1995) experiments.

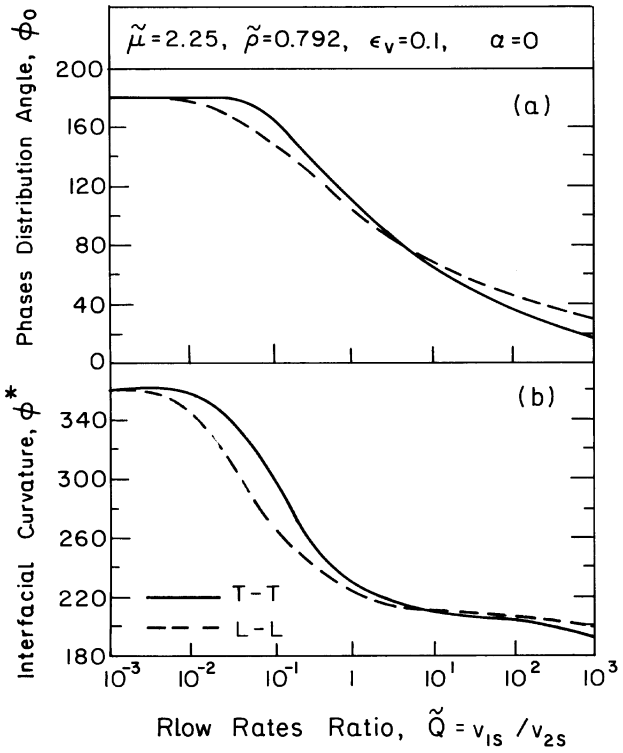

Fig. 8. Predicted interfacial structure: effect of phases flow rates and flow regime for ideal wettability of the water phase, $\alpha = 0$.

rates, the interface shape is determined by the corresponding ϕ_0 (Fig. 8a) and ϕ^* (Fig. 8b). Both ϕ_0 and ϕ^* vary moderately with laminar/turbulent flow regime transition.

It is to be noted that the range of operational conditions reported by Valle & Kvandal (1995) (oil: $U_{as} = 0.25 \div 1.05$ m/s, water: $U_{bs} = 0.2 \div 1.1$ m/s and $U_{as} + U_{bs} \leq 1.8$ m/s) correspond to turbulent flow in both phases. The relative phases velocities can be judged in view of Fig. 9. This figure shows the combinations of oil–water flow rates ratio and interfacial curvature, which result in a constant ratio of the *in situ* phases velocities. In the range of the reported experimental data ($0.2 < U_{as}/U_{bs} < 50$ and $\phi^* > 180^\circ$ in view of Fig. 8b) the phases velocities are of comparable levels ($0.5 < U_a/U_b < 2$). Therefore, the interfacial shear stress is modeled based on Eq. (5c). However, it is to be noted, that because of the relatively small velocity gap between the two phases, the particular model used for the interfacial friction factor has a minor effect on the predicted flow characteristics.

The solution obtained for ϕ_0 and ϕ^* for T–T flow (Fig. 8) determines the flow configuration for specified operational conditions. This solution is used to calculate the corresponding values of $\tilde{H}_f$ and $\tilde{H}_{50}$, which are compared with the experimental data in Fig. 10. The figure indicates that the model correctly predicts the location of the oil–water interface, as implied by the measurements of $\tilde{H}_f$ and $\tilde{H}_{50}$ and follows the observed effects of water and oil flow rates on the flow configuration. The interface curvature rises by increasing the water flow rate and/or reducing the oil flow rate, whereby a larger portion of the tube wall is lubricated by the water

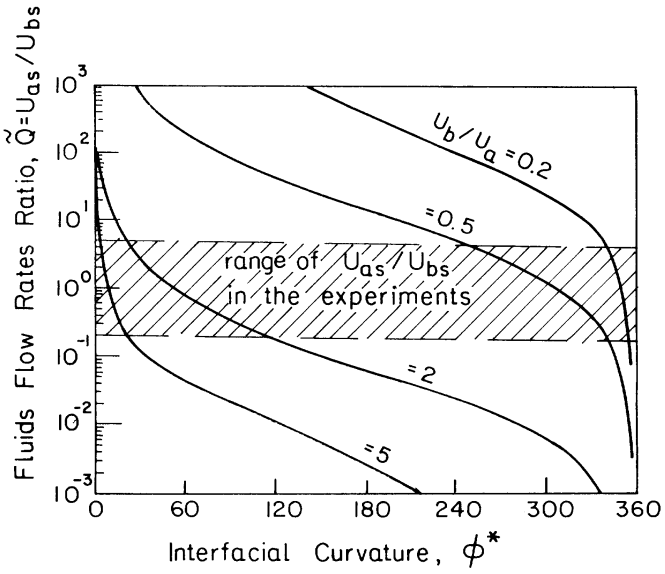

Fig. 9. Input flow rates ratio corresponding to constant ratio of the phases *in situ* velocities vs. the interfacial curvature (T–T flow, $\tilde{\mu}=2.25$, $\tilde{\rho}=0.792$).

and the flow gradually approaches a fully eccentric core-annular configuration. The greatest discrepancies of the model are at low oil flow rates and high water rates ($U_{as}\leq 25$ m/s, $U_{bs}\geq 1$ m/s), where the experiments indicate an evolution of eccentric annular flow—the water wets the entire tube surface with a large amount of water drops entrained in the oil phase and oil bubbles entrained in the water phase.

For comparison, the solution obtained for the water layer thickness assuming a planar interface $\tilde{H}^p$ is also indicated in Fig. 10(a) and Fig. 10(b). For plane interface $\tilde{H}^p=\tilde{H}^f=\tilde{H}_{50}$, and in view of Fig. 10, it is evident that a model of plane stratified flow fails to describe the flow configuration. The apparent reasonable agreement between the water-layer thickness H^p and the experimental values of H_{50} results from the mild sensitivity of the calculated value of $\tilde{H}_{50}$ (Eq. (14b)) to variation of the interface curvature; For specified flow rates, the decrease of $\tilde{H}_{50}$ with curving the water interface into a more concave shape is moderated, and sometimes even overruled by the associated increase of *in situ* water hold-up predicted for higher ϕ^*. Consequently, the minimal value of $\tilde{H}_{50}$ does not necessarily correspond to a fully eccentric core-annular configuration.

A comparison between the predicted pressure drop (associated with the predicted interface configuration) and the experimental data is shown in Fig. 11. In order to evaluate the effect of water lubrication, the pressure drop predicted via a plane interface model ($\phi^*=180°$) and that for a fully eccentric core configuration ($\phi^*=360°$) are also shown. For low oil flow rates and high water rates (Fig. 11a) the experimental pressure drop is not significantly different from that predicted with a plane interface, although the tube wall is shielded by a water film (Fig. 10(a)). The loss of water lubrication effect at low oil-flow rates is predicted by the model. However, a significant lubrication effect is noticed for high oil rates and low water rates. When relatively small amounts of water are introduced into an oil system, the potential for pressure

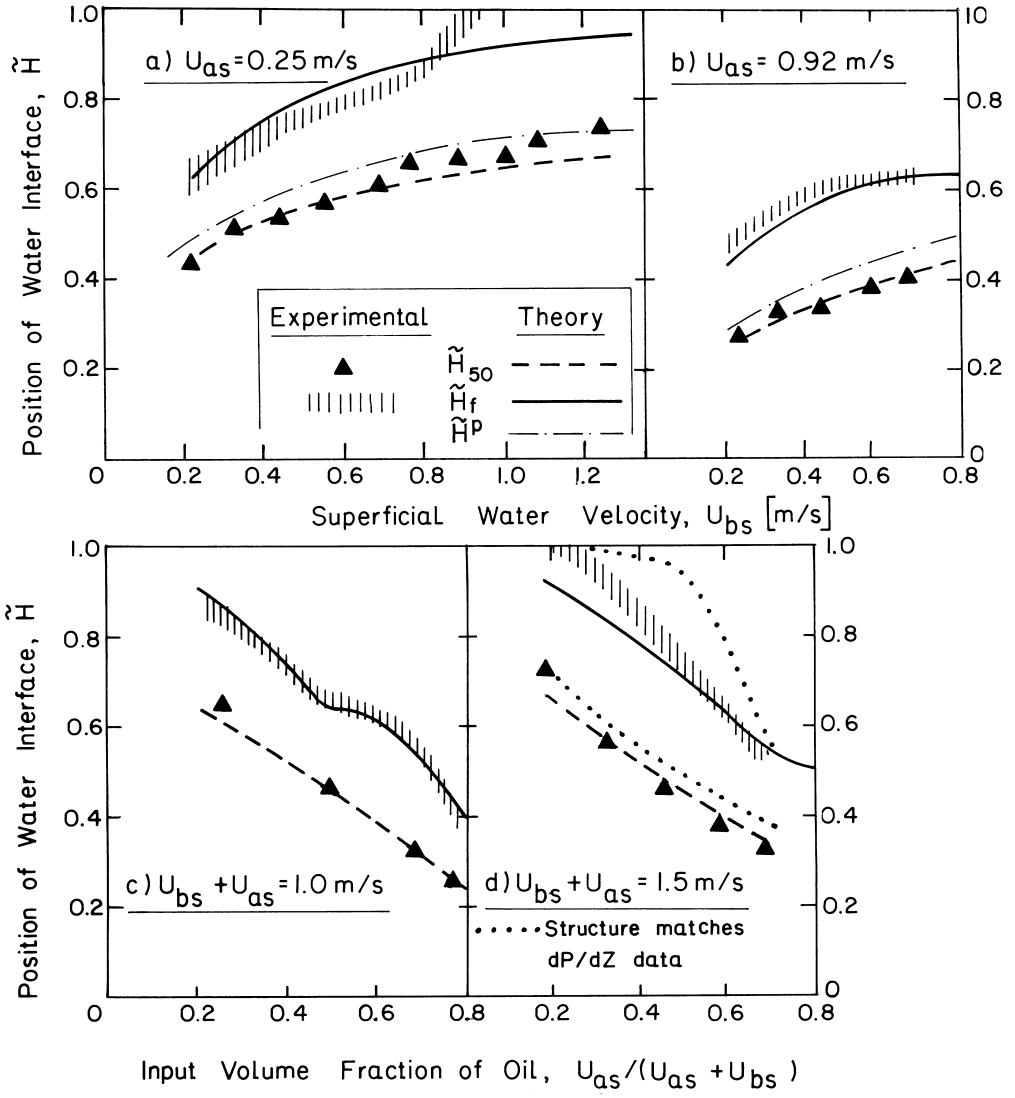

Fig. 10. Structure of oil–water interface—comparison of the model results with Valle and Kvandal (1995) experimental data.

drop reduction increases with changing of the interface configuration. A water lubrication effect can be achieved even when the water does not completely wet the tube wall. For instance, the interface configuration which yields a pressure drop matching the experimental data in Fig. 11(d), is depicted in Fig. 10(d) (dotted curves). Hence, water lubrication can be the cause of pressure drop reduction even in turbulent flows of two fluids of relatively low viscosity ratio.

Another possible mechanism for pressure drop reduction in turbulent two-phase flows, mentioned by Valle & Kvandal (1995), is the modification of the turbulent field due to the dynamics of droplets (bubbles) in unstable emulsions. This mechanism was suggested by Pal

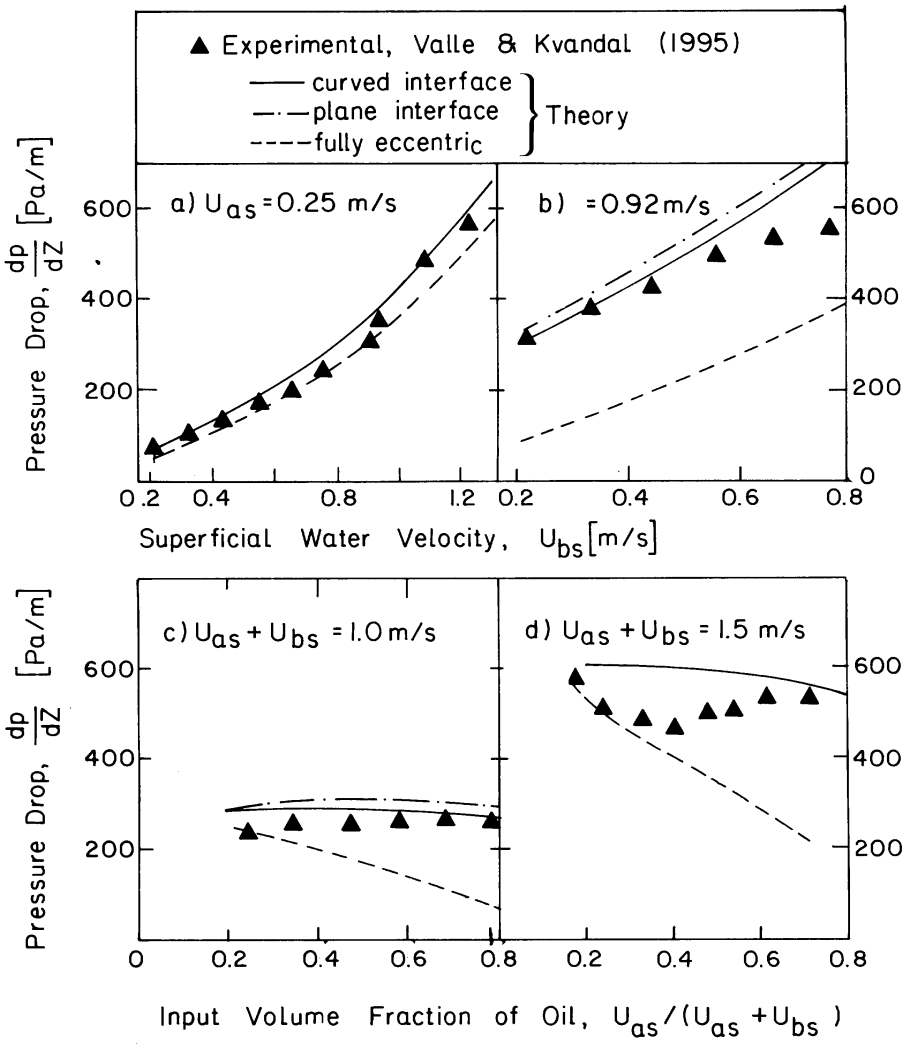

Fig. 11. Pressure drop in oil–water system–comparison of the model results with Valle and Kvandal (1995) experimental data.

(1993) to explain evidences of drag reduction in turbulent emulsions. It was substantiated by his experimental study, which indicated that the flow of surfactant-stabilized emulsion results in higher pressure drop in comparison to the otherwise unstable emulsion. It is, however, not clear to what extent the interference with turbulence in the near wall region is a valid mechanism for drag reduction by the relatively large drops observed in the stratified dispersed regime. This mechanism is attributed to the small drops ($1 \div 10\ \mu$m) which are encountered in emulsified oil–water systems. Valle and Kvandal data does not show consistent trends of increased drag reduction with increased entrainment. In particular, intensive entrainment of water drops into the oil phase at low oil-to-water flow rates ratio does not affect a pressure drop reduction. However, the loss of water lubrication under these

operational conditions is in accordance with the prediction of the curved interface two-fluid model.

It is to be noted that the interfacial structure predicted in Fig. 8 corresponds to ideal wettability of the glass surface by water ($\alpha = 0$). It is expected that other pipe materials with higher wettability angle, will affect the interfacial structure and reduce the potential for water lubrication. For example, the interfacial structure which is obtained from the 'operational monogram' of the same oil–water system of Fig. 8, but with ideal wettability of the oil phase ($\alpha = 180^\circ$), is shown in Fig. 12. The interfacial curvature is always less than 180°. Hence, the wall surface covered by water is always less than the calculation based on a model of stratified flow with a plane interface. However, the predicted pressure drop corresponding to the interfacial structure of Fig. 12 (not shown) is practically identical to that obtained for stratified flow with a plane interface.

6. Comparison of the two-fluid model with exact solutions

Analytical solutions for laminar stratified two-phase flow in pipes with a variable interfacial curvature have recently been presented by Brauner et al. (1995); Brauner et al., 1996b). The 2-D Navier–Stokes equations for the two-phases have been solved in the bipolar coordinates system (ϕ, ξ). The solution obtained for the velocity profiles is in the form of Fourier integrals:

$$\tilde{u}_a(\phi,\xi) = \frac{u_a}{U_R} = 2\sin\phi_0\left\{\frac{\sin(\phi-\phi_0)}{\cosh\xi-\cos\phi} + 2(1-\tilde{\mu})\frac{\sin(\phi^*-\phi_0)}{\sin(\phi^*)}\int_0^\infty W_{av}(\omega,\phi)\cos(\omega\xi)d\omega\right\};$$
$$\phi_0<\phi<\phi^*;\ \infty\le\xi\le\infty \tag{15a}$$

$$\tilde{u}_b(\phi,\xi) = \frac{u_b}{U_R} = 2\tilde{\mu}\sin\phi_0\left\{\frac{\sin(\phi-\phi_0)}{\cosh\xi-\cos\phi} + 2(1-\tilde{\mu})\frac{\sin(\phi^*-\phi_0)}{\sin(\phi^*)}\int_0^\infty W_{bv}(\omega,\phi)\cos(\omega\xi)d\omega\right\};$$
$$\phi^*<\phi<\phi_0+\pi;\ -\infty\le\xi\le\infty \tag{15b}$$

where:

$$U_R = \frac{-D^2}{16\mu_a}\frac{\partial p}{\partial z} \tag{15c}$$

and the spectral functions are given by:

$$W_{av}(\omega,\phi) = \frac{\sinh[\omega(\phi^*-\pi)]}{\psi(\omega)\sinh(\pi\omega)}\frac{\sinh[\omega(\phi-\phi_0)]}{\cosh[\omega(\phi^*-\phi_0)]} \tag{16a}$$

$$W_{bv}(\omega,\phi) = \frac{\sinh[\omega(\phi^*-\pi)]}{\psi(\omega)\sinh(\pi\omega)}\frac{\sinh[\omega(\phi-\pi-\phi_0)]}{\cosh[\omega(\phi^*-\pi-\phi_0)]} \tag{16b}$$

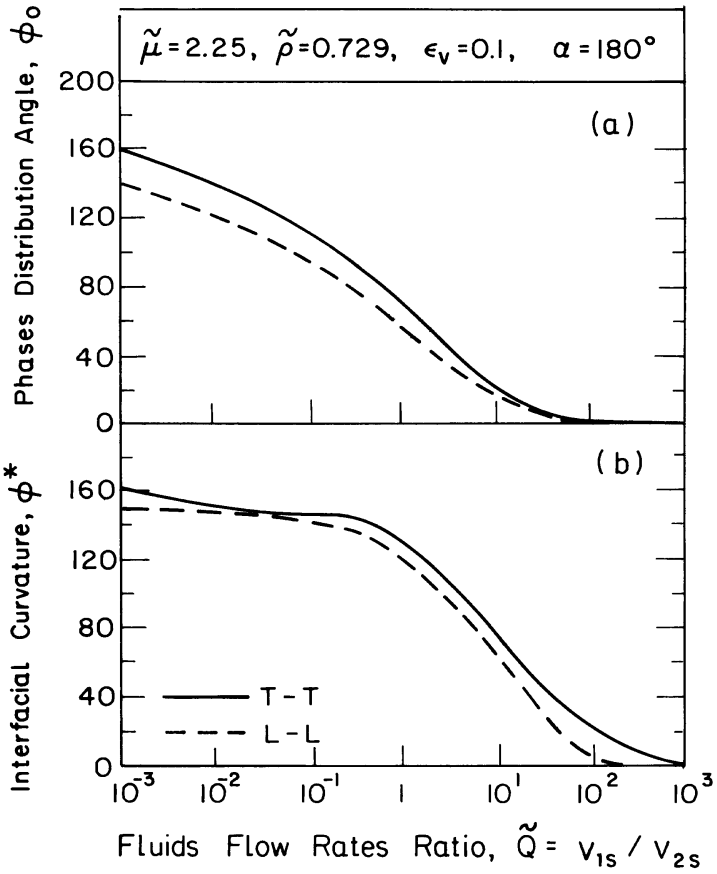

Fig. 12. Predicted interfacial structure—effect of phases flow rates and flow regime for ideal wettability of the oil phase ($\tilde{\alpha}=180°$).

where

$$\psi(\omega) = \tanh[\omega(\phi^* - \phi_0)] + \tilde{\mu}\tanh[\omega(\pi + \phi_0 - \phi^*)] \tag{16c}$$

Based on this solution, the velocity profiles, the distribution of wall and interfacial shear stress, pressure drop and *in situ* hold-up have been calculated for concave or convex interfaces ranging from an almost fully eccentric core of the lower phase (ϕ_0, $\phi^* \to 0$) to an almost fully eccentric core of the upper phase ($\phi^* \to 2\pi$, $\phi_0 \to \pi$).

Integration of the velocity profiles $\tilde{u}_a$, $\tilde{u}_b$ over the corresponding phases flow domains yields flow monograms of the form of Eq. (9a); namely a relation between ϕ_0 and ϕ^* for a specific flow rates ratio $\tilde{Q}$ and viscosity ratio $\tilde{\mu}$. For each particular point along the flow monogram (ϕ_0,ϕ^*), an exact solution for the dimensionless system pressure drop (corresponding to Eqs. (11a)–(c)) and *in situ* hold-up are also obtained.

Solutions for fully-eccentric core annular configurations cannot be obtained in the bipolar-coordinate system, since in this coordinate system flow domain of the annular phase degenerates to a line (either $\phi = 0$ or $\phi = 2\pi$). A special 'unipolar' coordinate system has

recently been used by Rovinsky et al. (1997) for solving the problem of fully eccentric core flows. The solutions for the velocity profiles in the core phase and annular phase, $\tilde{u}_c$ and $\tilde{u}_a$ respectively, were also obtained in the form of Fourier integrals:

$$\tilde{u}_a(\xi_1,\xi_2)=\frac{u_a}{\mathrm{U}_R}=\frac{4}{\xi_1^2+\xi_2^2}+\int_0^\infty W_a(\omega,\xi_2)\cos(\omega\xi_2)dw;\quad 1\le\xi_1\le\xi_c;\quad |\xi_2|<\infty \tag{17a}$$

$$\tilde{u}_c(\xi_1,\xi_2)=\frac{u_c}{U_R}=\frac{4\tilde{\mu}}{\xi_1^2+\xi_2^2}+\int_0^\infty W_c(\omega,\xi_2)\cos(\omega\xi_2)dw;\quad \xi_c\le\xi_1\le\infty;\quad |\xi_2|<\infty \tag{17b}$$

where:

$$\tilde{\mu}=\mu_a/\mu_c;\quad \xi_c=D/D_c \tag{18a}$$

$$U_R=\frac{-D^2}{16\mu_a}\frac{\partial p}{\partial Z} \tag{18b}$$

and the spectral functions W_a, W_c are given by:

$$W_a(\omega,\xi_1)=-\frac{4}{\xi_c}\frac{[(1-\tilde{\mu})e^{2(1-\xi_c)\omega}-(1+\tilde{\mu})\xi_c]+(1-\tilde{\mu})(\xi_c-1)e^{2\omega(\xi_1-\xi_c)}}{(1-\tilde{\mu})e^{2(1-\xi_c)\omega}-(1+\tilde{\mu})}e^{-\omega\xi_1} \tag{19a}$$

$$W_c(\omega,\xi_1)=\frac{4\tilde{\mu}}{\xi_c}\frac{[2\xi_c+\tilde{\mu}-1-(1-\tilde{\mu})e^{2(1-\xi_c)\omega}]}{[(1-\tilde{\mu})e^{2\omega(1-\xi_c)}-(1+\tilde{\mu})]}e^{-\omega\xi_1} \tag{19b}$$

Note that in Eqs. (17a)–(b), (18a)–(b) and (19a)–(b), subscript a denotes the annular phase. Integration of the velocity profiles over the corresponding core and annular flow domains yields a relation between the dimensionless core diameter (D_c/D) fluids flow rates ratio $\tilde{Q}=Q_a/Q_c$ and viscosity ratio, $\tilde{\mu}=\mu_a/\mu_c$ (Rovinsky et al., 1997).

The above exact solutions can be used to validate the two-fluid model. Fig. 13–15 demonstrate a comparison between the characteristics of laminar flow with curved interface as predicted via the two-fluid model with the corresponding results of the exact solutions for $\tilde{\mu}=8$. On each of the figures, the two-fluid model is represented by two curves—the SW curve represents the results obtained when the phases interface is considered as a solid wall with respect to faster phase. Hence Eq. (5a) or Eq. (5b) is used for modelling the interfacial shear. The FS curve represents the corresponding results when the interfacial shear is modeled assuming a free interface with respect to both phases, whereby Eq. (5c) applies.

Fig. 13 shows the variation of the dimensionless two-phase pressure drop with the interfacial curvature for various fluids flow rates ratio. The variation of the *in situ* hold-up is shown in Fig. 14 and the corresponding ratio of the average *in situ* phases velocities is shown in Fig. 15. Examination of these figures shows that when $\mathrm{U}_a\#\mathrm{U}_b$ (either $\mathrm{U}_a/\mathrm{U}_b\gg1$ or $\mathrm{U}_a/\mathrm{U}_b\ll1$ in Fig. 15) the predictions of the SW two-fluid model are in reasonable agreement with the results of the exact solutions over a wide range of operational conditions and interfacial curvatures associated with $\mathrm{U}_a\#\mathrm{U}_b$. Although the SW two-fluid model tends to overpredict the pressure

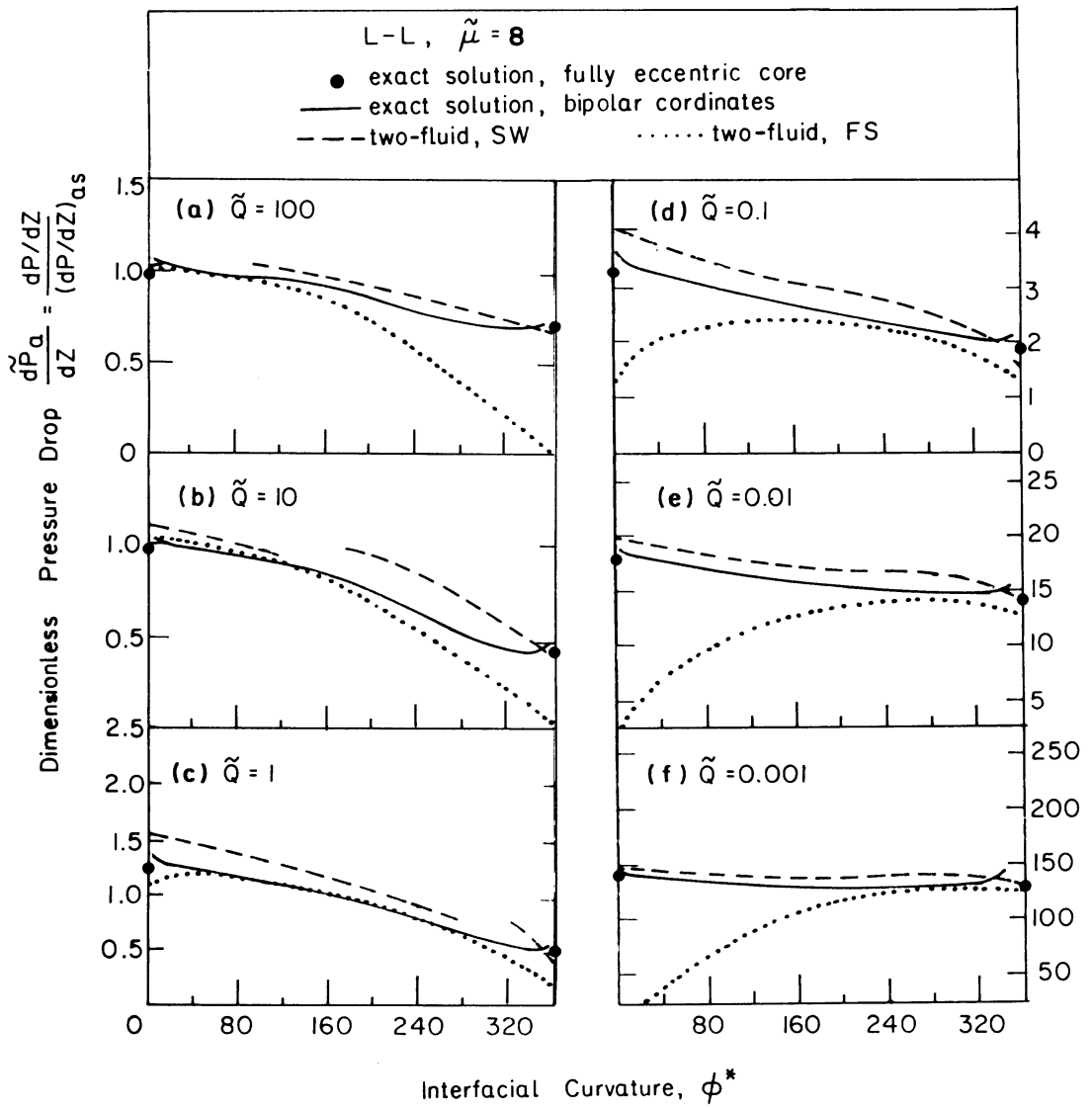

Fig. 13. Comparison of the results of the two-fluid model with the exact solution—pressure drop.

drop, it correctly predicts the *in situ* hold-up and the errors are most probably at an acceptable level for practical applications.

It is to be noted that for certain flow rates ratios there is a range of interfacial curvatures for which the velocities of the two phases are comparable, $U_a/U_b \simeq 1$ (Fig. 15). In this range the SW two-fluid model fails (no physical solution is reached) and the FS model must be applied (see Fig. 13(a–d)). In this range, the FS model provides a reasonable prediction of the system pressure drop and *in situ* hold-up. When the velocities of the two phases are of the same order of magnitude $0.1 < U_a/U_b < 10$, the difference between the prediction of the FS and SW two-fluid models diminishes. It is to be noted that in the range of comparable velocities, when the

lower less viscous phase is the faster phase ($0.1 < U_a/U_b < 1$), the FS model behaves better in predicting the system pressure drop. When the upper viscous phase is faster ($1 < U_a/U_b < 10$), the exact solution is in the middle of the predictions of and the FS model and the SW model.

Figs. 13–15 can also be used for demonstrating the effect of the interfacial curvature on the characteristics of laminar two-phase flows. The pressure drop in Fig. 13 is normalized with respect to the superficial pressure drop of the viscous phase. From a practical point of view, when the upper phase flow rate is maintained at a constant value (and so $(\partial p/\partial z)_{as}$) this nondimensional pressure drop yields the factor of pressure drop reduction (or enhancement) associated with introducing a second less viscous phase to the system. Indeed, Fig. 13

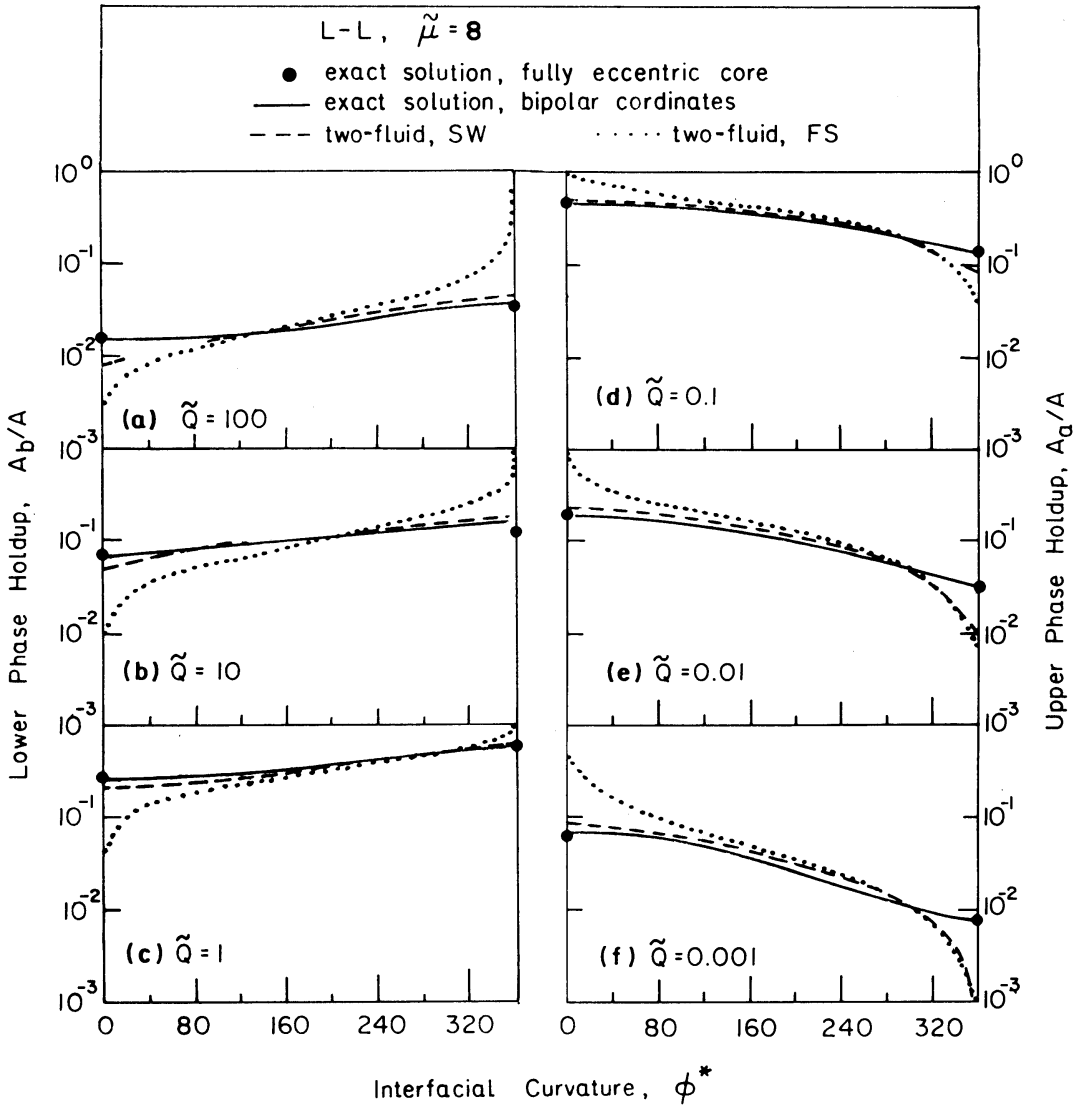

Fig. 14. Comparison of the results of the two-fluid model with the exact solution—*in situ* hold-up.

demonstrates that for $\tilde{\mu}=8$, a reduction of the system pressure drop can be achieved by adding relatively small amounts of less viscous phase ($Q_a/Q_b>1$). The reduction is more significant as ϕ^* (and ϕ_0 as well) increases and the interface attains a concave shape, whereby the lower less viscous phase spreads over an increasing portion of the tube wall. Note that for a plane interface, $\phi^*=180°$, the maximal achievable pressure drop reduction for this viscosity ratio is limited to about 20%. By reducing Q_a/Q_b (increasing the flow rate of the less viscous phase) the two-phase pressure drop eventually increases and for $Q_a/Q_b<\sim 0.3$, an enhancement of the pressure drop results independently of the interface configuration. Fig. 14 shows that the *in situ*

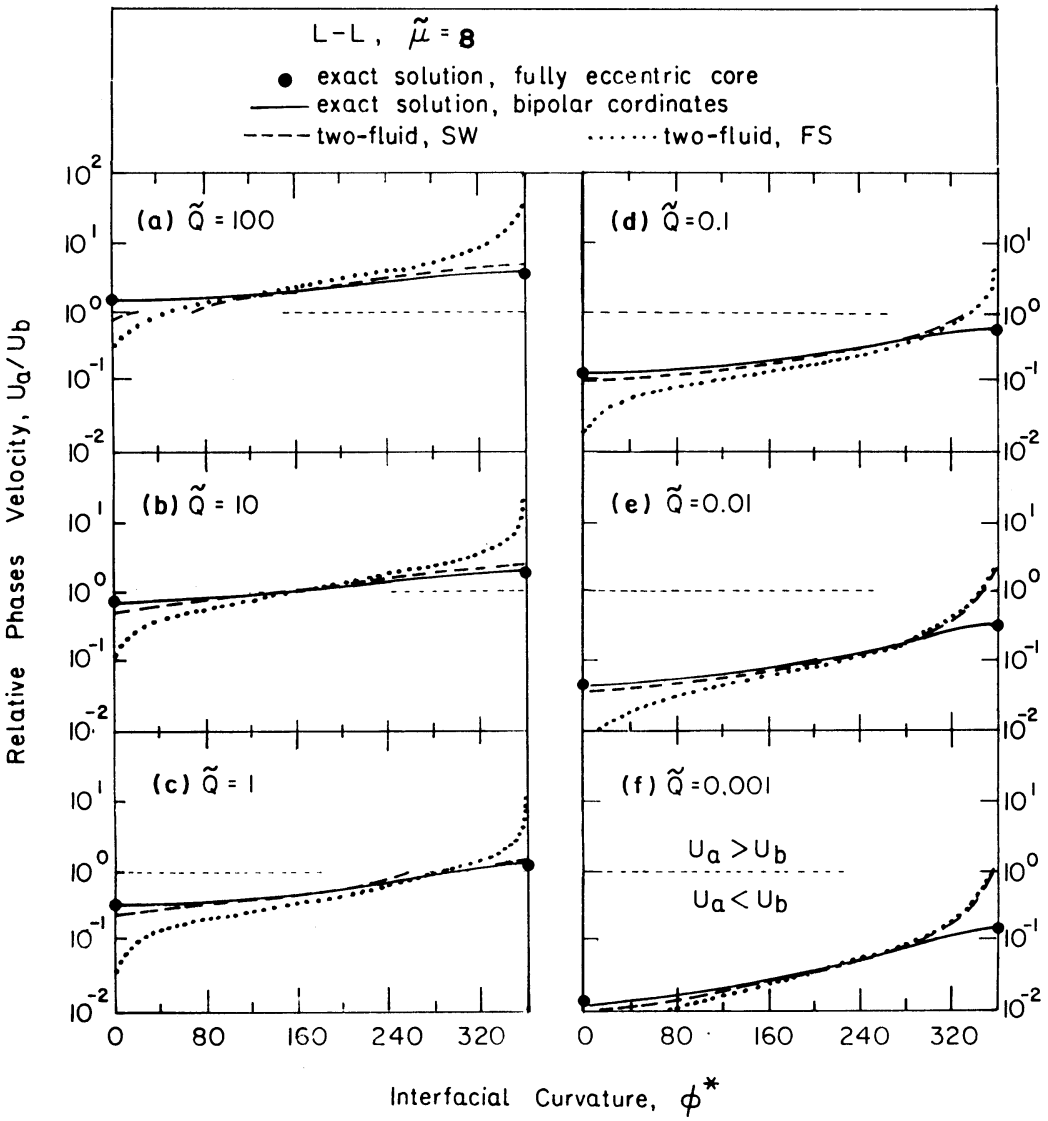

Fig. 15. Comparison of the results of the two-fluid model with the exact solution—relative velocities of the two-phases.

hold-up of the less viscous phase increases by increasing the interface curvature, resulting in a corresponding increase of the phases velocity ratio (Fig. 15).

The solutions for the fully eccentric core-annular configuration at $\phi_0 = 0 (\phi^* = 0)$ and $\phi_0 = \pi (\phi^* = 2\pi)$ are also marked in Figs. 13–15. One can observe that the exact solutions for curved interfaces obtained in the bipolar coordinate system do not converge to the pressure drop and *in situ* hold-up values obtained for the fully eccentric core-annular configuration. The characteristics of laminar stratified flows when approaching the limit of fully eccentric core-annular configuraton have been discussed by Brauner et al. (1997); The solution in the bipolar coordinate system yields a lower hold-up (and higher velocity) of the core phase, which results in higher pressure drop compared to the values predicted by the solution obtained for a fully eccentric core. This rather peculiar behavior in the extremes of ($\phi^* \to 0^\circ$ and $\phi^* \to 360^\circ$) may evolve from computational problems due to the limitations of the bipolar coordinate system when approaching the limits of its applicability (Rovinsky et al., 1997). Nevertheless, these trends in the solutions remain invariant with the system parameters ($\tilde{\mu}$ and $\tilde{Q}$) and the change in the computational tolerances.

It is worth noting that the reasonable agreement between the prediction of the two-fluid model and the exact solution at the limit of a fully eccentric core, as implied by Fig. 15, may be misleading. The results of the two-fluid model, when applied to annular configuration, are invariant with respect to the core eccentricity. This is an obvious outcome of using closure laws for the shear stresses which ignore the core position and are uniquely determined by the core phase hold-up.

The effect of the core eccentricity on the pressure drop (and hold-up) has recently been studied by Rovinsky et al. (1997) in view of the exact solution obtained for a fully eccentric core flow. It was shown that in viscous core flow, $\mu_c/\mu_a > 1$, the pressure drop in concentric configuration is always lower than that of an eccentric configuration. But significant effects of the core eccentricity are limited to the lubrication region $0 < (\mu_a Q_a)/(\mu_c Q_c) < 1$ (where pressure drop reduction is achieved by introducing a second less viscous phase). In the lubrication region, the pressure drop factor with a concentric core is proportional to μ_a/μ_c and for $\mu_a/\mu_c \to 0$, $d\tilde{P}_c/dZ \to 0$; whereas with a fully eccentric core, the minimal pressure drop factor is still obtained for $\mu_a/\mu_c \to 0$, but is bounded by 0.025. The maximal effect of core eccentricity was shown to be in the range $0.1 < Q_a/Q_c < 10$, independent of the viscosity ratio (see Fig. 8 in Rovinsky et al., 1997). It was also shown that the viscous core hold-up predicted for a concentric core underestimates the hold-up of a core at a eccentric position. This is expected since the proximity of the tube wall slows down the viscous core and a higher flow area is needed to transfer the core phase input flow rate. In contrast to concentric annular flows, where the average velocity of the annular phase is always smaller than the average velocity of the core phase (independent of the fluids viscosity ratio and flow rates), in eccentric core flows, the annular phase velocity may exceed the core velocity. For $\tilde{\mu} = \mu_a/\mu_c \ll 1$ the annular phase is the faster one (except for $\tilde{Q} = Q_a/Q_c \ll 1$, Fig. 7, Rovinsky et al., 1997). However, in the range of operational conditions, which are relevant for viscous core lubrication, the effect of core eccentricity on the *in situ* hold-up was found to be moderate.

In view of the limitations of the two-fluid model in accounting for the core eccentricity, the error in predicting the lubrication effect in the limit of $\phi^* \to 360^\circ$ are scaled with the viscosity ratio. For $\mu_a/\mu_b = 8$ (used in Fig. 13), the two-fluid model underpredicts the pressure drop. The

maximal error (normalized with respect to the pressure drop of concentric core) is about 25% for $Q_a/Q_b = 1$ and can be practically ignored for $Q_a/Q_b > 100$ or $Q_a/Q_b < 0.01$.

However, for $\mu_a/\mu_b = 100$ for instance (Fig. 16), the maximal error increases; it amounts to $\approx$250% for $Q_a/Q_b = 1$ and the range of flow rates associated with a significant error ($> 5\%$) is wider ($2 \times 10^{-3} < Q_a/Q_b < 2 \times 10^3$). Consistent with the above discussion, Fig. 14 indicates that the two-fluid model underpredicts the viscous core hold-up (and overpredicts its velocity, Fig. 15), but the large errors indicated in Fig. 14(d–f)Fig. 15(d–f) are for low $\tilde{Q}$ where the core phase hold-up is very low and no lubrication effect can be achieved ($d\tilde{P}_a/dZ > 1$ in Fig. 13(d–f)).

The other extreme of $\phi^* \rightarrow 0$ in Figs. 13–15 corresponds to a fully eccentric core of the less viscous phase. The exact solution for this configuration (Rovinsky et al., 1997) yields a pressure drop which is lower than the value corresponding to a concentric core. But, the variation due to the core eccentricity was shown to be limited to 35% (approached for high $\tilde{\mu}$).

Hence, the extent of agreement of the two-fluid model with the exact solution, as shown in Figs. 13–15 for $\tilde{\mu} = 8$ and various ϕ^*, practically applies for any $\tilde{\mu}$, except when the flow configuration approaches that of a fully eccentric viscous core ($\phi^* \rightarrow 360$ for $\tilde{\mu} \gg 1$, or $\phi^* \rightarrow 0$ for $\tilde{\mu} \ll 1$).

7. Conclusion

The vast majority of stratified two-phase models assume that a plane interface is the basic configuration. This study shows that in many practical two-phase systems, when the assumption of a plane interface is relaxed, the fluids interface attains a concave or convex shape.

In previous studies (Brauner et al., 1995, 1996a; Rovinsky et al., 1997), exact analytical solutions for the two-dimensional velocity profiles in laminar stratified flows with curved interfaces were obtained. For practical applications, however, it is necessary to have a model which can also handle turbulent flows and mixed-flow regimes in the two phases.

In this study, a two-fluid model is used for modelling stratified flows with curved interfaces. The solutions of the two-fluid model are used to construct 'flow monograms' which provide a relation between a specified interface curvature and the *in situ* hold-up under given operational conditions. A closure relation for determining the interface curvature is obtained by invoking the principle of minimal total system energy (sum of potential and surface energies). The closure relation is represented by an interface monogram.

The combination of the system 'interface monogram' with the system 'flow monogram' yields an 'operational monogram', which provides a complete solution for the flow problem. The solution includes the interface shape, *in situ* hold-up and the associated pressure drop. The construction of operational monograms is demonstrated for laminar, turbulent or mixed flow regimes in the two-phases, for horizontal and inclined systems. The information needed for constructing the system operational monogram is defined in terms of nondimensional input parameters. It includes the ratio of the fluids input flow rates, viscosity ratio, density ratio, wall/phases adhesion (wettability angle) and the Eötvös number. The latter represents the ratio of surface tension and gravity forces, as determined by the fluids surface tension, density

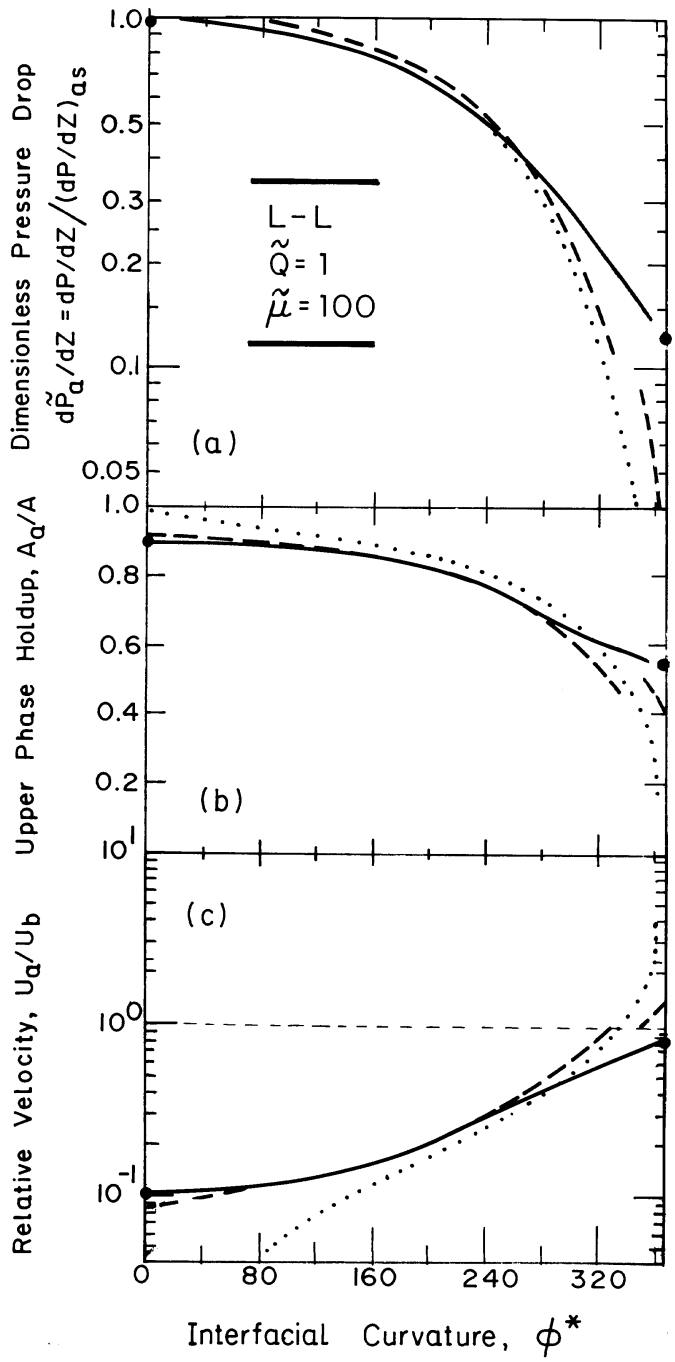

Fig. 16. Comparison of the results of the two-fluid model with the exact solution for $\tilde{\mu}=100$; $\tilde{Q}=100$ (curves notation as in Figure 15).

differential, tube diameter and gravitational field. For mixed flow regime and inclined systems, the Reynolds number of either one of the phases should also be provided. It is shown that the interface curvature may significantly affect the stratified flow characteristics.

Experimental data obtained by Valle & Kvandal (1995) for stratified flow of an oil–water system is used to verify the model. The comparisons with the experimental data of the *in situ* flow configuration and the corresponding pressure drop highlight the potential offered by the model to improve the predictions of stratified flow characteristics in liquid–liquid systems and other two-fluid systems of a nonvanishing Eötvös number.

The accuracy of the model and its limitations are tested by comparing its predictions, when applied for laminar flows, with the corresponding exact solutions (Brauner et al., 1995; Rovinsky et al., 1997). The comparison shows that the two-fluid model provides a reasonable estimate of the *in situ* hold-up and pressure drop over a wide range of interfacial curvature and flow rates. The biggest errors are obtained when the two fluid model is applied for a configuration of a fully eccentric highly viscous core, in which case the two-fluid model significantly overpredicts the lubrication effect of the less viscous phase.

It should be noted, however, that the inherent limitations of the two-fluid model in reflecting the consequences of variations of the velocity profiles are expected to be pronounced mostly in laminar flows. It can be speculated that for turbulent flows the accuracy of the two-fluid model may turn out to be even better.

References

Agrawal, S. S., Gregorif, G. A., Govier, G. W., 1973. An analysis of horizontal stratified flow in pipes. Can. J. Chem. Engng. 51, 280–286.

Bentwich, M., 1964. Two-phase axial flow in pipe. Trans. of the ASME, Series D 86 (4), 669–672.

Brauner, N., Moalem Maron, D., 1989. Two-phase liquid–liquid stratified flow. Physico-Chem. Hrdrodynam. 11, 487–506.

Brauner, N., Rovinsky, J., Moalem Maron, D., 1995. Analytical solution of laminar stratified flow with curved interfaces. Proceedings of the NURETH-7 Meeting, ANS 1, 192–211.

Brauner, N., Rovinsky, J. & Moalem Maron, D., 1996a. Analytical solution for Laminar–Laminar two-phase flow in circular conduits. Chem. Eng. Comm. A. Dukler memorial issue, 141-142, 103-143.

Brauner, N., Rovinsky, J., Moalem Maron, D., 1996b. Determination of the interface curvature in stratified two-phase systems by energy considerations. Int. J. Multiphase Flow. 22, 1167–1185.

Brauner, N., Rovinsky, J. & Moalem Maron, D., 1997. Characteristics of annular and stratified two-phase flows in the limit of fully eccentric core annular configuration. Proc. of the ExHFT 4, Brussels, June 2–6, (1997) (Edited by M. Giot, Mayinger and C. P. Celata), 2, 1189-1196.

Charles, M. E., 1960. The reduction of pressure gradients in oil pipelines: experimental results for the stratified flow of heavy crude oil and water. Can. Inst. Min. Metal. Trans. 63, 306–310.

Charles, M. E., Redberger, P. J., 1962. The reduction of pressure gradients in oil pipelines by the addition of water: Numerical analysis of stratified flow. Can. J. Chem. Engng. 40, 70–75.

Gemmell, A. R., Epstein, N., 1962. Numerical analysis of stratified laminar flow of two immiscible Newtonian liquids in a circular pipe. Can. J. Chem. Engng. 40, 215–224.

Hall, A. R., Hewitt, G. F., 1993. Application of two-fluid analysis to laminar stratified oil–water flows. Int. J. Multiphase Flow 19 (4), 711–717.

Moalem Maron, D., Rovinsky, J. & Brauner, N., 1995. Analytical prediction of the interface curvature and its effects on stratified flow characteristics. Proc. of the Int. Symp. on two-phase flow modeling and experimentation, Vol. 1, edited by G. P. Celata and R. K. Shah, Edizioni ETS, pp. 163–170.

Pal, R., 1993. Pipeline flow of unstable and surfactant stabilized emulsions. A.I.Ch.E. Journal 39, 1754–1764.

Rovinsky, J., Brauner, N., Moalem Maron, D., 1997. Analytical solution of laminar two-phase flow in the limit of fully eccentric core-annular configuration. Int. J. Multiphase Flow. 23, 523–543.

Russell, T. W. F., Charles, M. E., 1959. The effect of the less viscous liquid in the laminar flow of two immiscible liquids. Can. J. Chem. Engng. 37, 18–34.

Russell, T. W. F., Hodgson, G. W., Govier, G. W., 1959. Horizontal pipeline flow of mixtures of oil and water. Can. J. Chem. Engng. 37, 9–17.

Taitel, Y., Dukler, A. E., 1976. A model for prediction flow regime transition in horizontal and near horizontal gas–liquid flow. A.I.Ch.E. J. 22, 47–55.

Tang, Y. P., Himmelblau, D. M., 1963. Velocity distribution of isothermal two-phase co-current laminar flow in horizontal rectangular duct. Chem. Engng. Sci. 18, 143–144.

Valle, A. & Kvandal, H. K., 1995. Pressure drop and dispersion characteristics of separated oil–water flow. Proc. Int. Symp. on two-phase flow modeling and experimentation, Vol. 1, Oct. 9–11, Rome, Italy, edited by G. P. Celata and R. K. Shah, Edizioni ETS, pp. 583–591.

Wang, C. C., Charles, M. E., 1981. Co-current stratified flow of immiscible liquids; velocity distribution and pressure gradient in the laminar–laminar and laminar–turbulent regimes. Can. J. Chem. Engng 59, 669–676.

Yu, H. S., Sparrow, E. M., 1967. Stratified laminar flow in ducts of arbitrary shape. A.I.Ch.E. Journal 13, 10–16.